Multifactorial seroprofiling dissects the contribution of pre-existing human coronaviruses responses to SARS-CoV-2 immunity

Irene A. Abela[1,2$], Chloé Pasin[1,2$], Magdalena Schwarzmüller[1$], Selina Epp[1], Michèle E. Sickmann[1], Merle M. Schanz[1], Peter Rusert[1], Jacqueline Weber[1], Stefan Schmutz[1], Annette Audigé[1], Liridona Maliqi[1], Annika Hunziker[1], Maria C. Hesselman[1], Cyrille R. Niklaus[1], Jochen Gottschalk[3], Eméry Schindler[3], Alexander Wepf[4], Urs Karrer[5], Aline Wolfensberger[2], Silvana K. Rampini[6], Patrick M. Meyer Sauteur[7], Christoph Berger[7], Michael Huber[1], Jürg Böni[1], Dominique L. Braun[1,2], Maddalena Marconato[8], Markus G. Manz[8], Beat M. Frey[3], Huldrych F. Günthard[1,2*], Roger D. Kouyos[1,2*], Alexandra Trkola[1*]

[$]these authors contributed equally

[*]these authors contributed equally

trkola.alexandra@virology.uzh.ch

Huldrych.Guenthard@usz.ch

Roger.Kouyos@usz.ch

Affiliations

[1] Institute of Medical Virology, University of Zurich, Switzerland

[2] Division of Infectious Diseases and Hospital Epidemiology, University Hospital Zurich, Switzerland

[3] Blood Transfusion Service Zurich, Switzerland

[4] Institute of Laboratory Medicine, Cantonal Hospital Winterthur, Switzerland

[5] Department of Medicine, Cantonal Hospital Winterthur, Switzerland

[6] Department of Internal Medicine, University Hospital Zurich, Switzerland

23 [7] Division of Infectious Diseases and Hospital Epidemiology, University Children's Hospital Zurich,
24 Switzerland

25 [8] Department of Medical Oncology and Hematology, University Hospital and University of Zurich,
26 Switzerland

27

28

Abstract

Determination of SARS-CoV-2 antibody responses in the context of pre-existing immunity to circulating human coronavirus (HCoV) is critical to understanding protective immunity. Here we perform a multifactorial analysis of SARS-CoV-2 and HCoV antibody responses in pre-pandemic (N=825) and SARS-CoV-2-infected donors (N=389) using a custom-designed multiplex ABCORA assay. ABCORA seroprofiling, when combined with computational modeling, enables accurate definition of SARS-CoV-2 seroconversion and prediction of neutralization activity, and reveals intriguing interrelations with HCoV immunity. Specifically, higher HCoV antibody levels in SARS-CoV-2-negative donors suggest that preexisting HCoV immunity may provide protection against SARS-CoV-2 acquisition. In those infected, higher HCoV activity is associated with elevated SARS-CoV-2 responses, indicating cross-stimulation. Most importantly, HCoV immunity may impact disease severity, as patients with high HCoV reactivity are less likely to require hospitalization. Collectively, this evidence points to HCoV immunity promoting the rapid development of SARS-CoV-2-specific immunity, underscoring the importance of exploring cross-protective responses for comprehensive coronavirus prevention.

45 **Introduction**

46 Monitoring the antibody response to SARS-CoV-2 is critical to define correlates of vaccine protection,
47 differences in susceptibility to infection and in disease severity. The picture of the antibody landscape
48 to SARS-CoV-2 that has thus far evolved is complex. The antibody response to SARS-CoV-2 is rapid, and
49 triggers strong IgM, IgA and IgG responses [1,2]. Both binding and neutralizing responses increase with
50 disease severity and show in part dependence on demographic parameters such as age and gender [3-
51 5]. It remains, however, unclear which factors are independent drivers of antibody responses, reflect
52 severe disease courses or are confounded by other factors including infection length and co-
53 morbidities. Waning IgG binding and neutralizing antibody titers may be particularly pronounced in
54 individuals with asymptomatic or mild infection [6-9]. IgG responses to spike (S) glycoprotein may persist
55 longer than to nucleocapsid protein (N) [7,10,11] and can in part undergo affinity maturation post virus
56 clearance [5]. Current serological analyses predominantly focus on measuring reactivity to N, the spike
57 glycoprotein S1 subunit and the ACE2 receptor-binding domain (RBD) in S1 [2,5,12-16]. Antibodies to RBD
58 and the receptor-binding motif within the RBD constitute the main group of neutralizing antibodies,
59 followed by S1 trimer specific, spike N-terminal domain, and spike S2 neutralizing antibodies [16-22]. S1
60 and RBD binding correlate with neutralizing activity in both natural and vaccine-induced immune
61 responses providing means to estimate the potential for neutralization where neutralization capacity
62 cannot be assessed directly [6,8,10]. Considering the complex antibody response patterns, possibilities to
63 capture the dynamics of the SARS-CoV-2 response across diverse Immunoglobulin (Ig) classes and
64 SARS-CoV-2 antigens are needed to ascertain sensitive detection of seroconversion and sero-reversion
65 and to establish links to protective, neutralizing activity post infection and post vaccination.

66 Infections with circulating human coronaviruses (HCoV), alphacoronavirus (HCoV-229E, HCoV-NL63)
67 and betacoronavirus (HCoV-HKU1, HCoV-OC43), are common and contribute considerably to the
68 seasonal respiratory disease burden in humans [23,24]. Despite an overall modest sequence homology
69 between SARS-CoV-2 and circulating HCoVs, several conserved regions exist and antibody cross-
70 reactivity may occur [25-27]. While dismissed in the diagnostic setting as false-positives [28], cross-reactive

71 antibodies may bear biological relevance as suggested for SARS-CoV-2 S2 cross-neutralizing antibodies
72 [29]. Uncertainty remains, however, whether cross-reactive HCoV antibody responses influence the
73 evolution of SARS-CoV-2 specific immunity. Positive impact by providing early low affinity memory
74 responses to build on and mature as well as negative influences following the antigenic sin principle [30]
75 by boosting non-protective cross-reactive antibodies on the expense of de-novo responses can be
76 envisaged. Of particular note, cross-reactive HCoV T helper cell responses were shown to positively
77 impact SARS-CoV-2 specific immunity [31]. In view of this, the definition of pre-existing immunity due to
78 prior infection with HCoVs will become important in clinical diagnosis and strategies to record and
79 unveil the complex interdependencies HCoV and SARS-CoV-2 responses side by side are needed to fill
80 this knowledge gap.

81 Here we report on the development of a serological assay that allows multifactorial seroprofiling of
82 SARS-CoV-2 and HCoV responses at high diagnostic accuracy. Seroprofiling of a large cohort of SARS-
83 CoV-2 infected and uninfected individuals provided key insights into the interdependencies of HCoV
84 and SARS-CoV-2 antibody responses. The results highlight a potential protective role of HCoV-specific
85 responses in SARS-CoV-2 acquisition as well as in shaping the SARS-CoV-2 response upon infection.

86

87

88 **Results**

89 **Multifactorial seroprofiling defines SARS-CoV-2 specific responses**

90 Recognizing the need for comprehensive SARS-CoV-2 serological profiling to elucidate central
91 questions in SARS-CoV-2 immunity and its interdependencies with HCoV responses, we created a bead-
92 based multiplex immunoassay to measure specific IgG, IgA and IgM responses to SARS-CoV-2 RBD, S1,
93 S2 and N (Supplementary Fig. 1). The assay records in total 12 SARS-CoV-2 specific antibody parameters
94 (4 antigens across 3 Ig classes) with high diagnostic accuracy (see methods, Supplementary Fig. 1-3 and
95 Supplementary Tables 1, 2) and further includes the S1 protein of HCoV-HKU1 to screen cross-reactive
96 antibodies alongside SARS-CoV-2 responses. According to the test's design to monitor antibodies to
97 two coronaviruses, we termed the assay AntiBody CORonavirus Assay (ABCORA) 2.0.
98 Measurements in ABCORA are expressed as median fluorescence intensity (MFI) corrected for
99 background binding (fold over empty beads, FOE). To distinguish SARS-CoV-2-specific from cross-
100 reactive antibodies, we defined MFI-FOE thresholds for each of the 12 SARS-CoV-2 antigen and Ig class
101 combinations based on plasma antibody reactivity in training cohorts of pre-pandemic healthy donors
102 (Training I, N=573), donors with recent HCoV infection (Training II, N= 75) and donors with confirmed
103 SARS-CoV-2 infection (Training III, N=175) (Fig. 1a, Supplementary Table 3). Positive call criteria were
104 defined to ascertain that in at least two of the 12 antigen and Ig combinations the threshold is reached
105 (Supplementary Table 4). The final threshold and positive call criteria allowed for a differentiation of
106 partial (only IgM and IgA responses) to full seroconversion (including IgG responses). In addition, the
107 criteria denote samples with weak reactivity and/or indeterminate reactivity (Supplementary Table 5).

108 Pre-pandemic patients with documented, recent HCoV infection (Training II, N=75; OC43 (N=27), HKU1
109 (N=17), NL63 (N=22), 229E (N=9)) comprised individuals with different underlying severe diseases
110 including immune compromised patients that underwent diagnostic screening for HCoV. HCoV specific
111 activity was overall lower in this syndromic group but showed, as expected, enriched HCoV reactivity
112 against the infecting HCoV (Supplementary Fig.4). Importantly, we observed no indication of cross-

113 reactivity with SARS-CoV-2 antigens that affects the ABCORA readout (Fig. 1a, b). Considering data of
114 all training cohorts (I-III), ABCORA 2.0 exhibited a high sensitivity and specificity, reaching 94.29%
115 sensitivity and 99.07% specificity (Fig. 1c, Supplementary Table 3).

116 To enable an analysis of cross-reactivities and interdependencies between SARS-CoV-2 and HCoV
117 antibodies, we recorded reactivity to the S1 unit of HCoV-HKU1 in addition to the SARS-CoV-2 antigens
118 (Fig. 1a). Owing to the high prevalence of HCoV antibodies and the ensuing lack of true-negative
119 controls, we set no thresholds to rate HKU1 reactivity as positive/negative. Overall, SARS-CoV-2 cross-
120 reactivity was low in pre-pandemic samples despite notable HKU1 activity (Fig. 1a). Correlation analysis
121 revealed modest interdependencies of SARS-CoV-2 and HKU1 plasma antibody reactivity in SARS-CoV-
122 2 positive and pre-pandemic donors. This predominantly involved IgM responses, with individuals with
123 recent HCoV infection showing the highest correlation in IgM for HKU1 and SARS-CoV-2 activity
124 (Supplementary Fig. 5). These data underline that a low level of cross-reactive activity exists that needs
125 to be respected in assay design, analysis and validation.

126 Verification of ABCORA 2.0 on separate validation cohorts of pre-pandemic healthy adults (N=252),
127 pre-pandemic children (N=169) and individuals with documented SARS-CoV-2 infection (N=214) (Fig.
128 1a, b, Supplementary Table 3) confirmed the validity of the chosen assay criteria. Combining training
129 and validation cohorts of SARS-CoV-2 positive individuals (N=389) and negative controls (N=825),
130 ABCORA 2.0 achieved a sensitivity of 94.60% and a specificity of 99.16% (Fig. 1c).

131 Of note, when analyzing children and adults in the validation cohort separately, we observed a slightly
132 lower specificity amongst children (98.82%) compared to adults (99.60%), raising the possibility that
133 cross-reactive activity in children may be more prevalent than in adults. Indeed, pre-pandemic children
134 showed a higher correlation of IgM HKU1 and SARS-CoV-2 (Supplementary Fig. 5c), highlighting that
135 interpretation of IgM SARS-CoV-2 activity can be complex.

136

137

138 **Computational analyses maximize specificity and sensitivity of SARS-CoV-2 seroprofiling**

139 To further increase specificity of the readout, we next explored two computational analysis extensions,
140 a logistic regression model (ABCORA 2.1) and a random forest model (ABCORA 2.2). Both analysis
141 strategies were established on the identical training dataset (Training I–III) used for the setup of
142 ABCORA 2.0. Instead of obtaining 12 individual thresholds (one per antigen and Ig class), the
143 computational models solely estimate the probability of a sample to be positive by providing a
144 composite result across all 12 measurements and ranking sera positive or negative (1, 0 classification).
145 For the logistic regression ABCORA 2.1, we grouped SARS-CoV-2 binding activities displaying high
146 correlation (Supplementary Fig. 6a) and included the mean value of their MFI-FOEs in the model. The
147 random forest model ABCORA 2.2 included all 12 SARS-CoV-2 responses measured and aggregated the
148 result of 1000 classification trees. On the combined training and validation cohorts of SARS-CoV-2
149 positive individuals (N=389) and negative controls (N=825), ABCORA 2.2 achieved a striking sensitivity
150 of 97.43% and a specificity of 99.91% outperforming both ABCORA 2.0 and 2.1. Of note, positive calling
151 by ABCORA 2.2 was dominated by IgG responses (Supplementary Fig. 6b).

152 We next explored whether incorporation of HKU1 reactivity into the random forest model may further
153 improve the calling specificity and sensitivity. Indeed, a model that included HKU1 S1 as additional
154 variable (ABCORA 2.3) increased sensitivity from 97.43% in ABCORA 2.2 to 98.20% (Fig. 1c,
155 Supplementary Table 3) without reduction of the specificity. A sensitivity cross-validation analysis with
156 randomized training and validation set confirmed the performance of ABCORA 2.3 (Supplementary
157 Table 6). Owing to its combined high sensitivity and specificity, we therefore selected ABCORA 2.3 as
158 the analysis strategy for rating global SARS-CoV-2 seroconversion.

159 We next verified the accuracy of ABCORA 2.0 and 2.3 in defining positive and negative SARS-CoV-2
160 immune status utilizing the National Institute for Biological Standards and Control (NIBSC) Anti SARS-
161 CoV-2 Verification Panel (20/B770) [32]. This verification panel for serology assays includes 23 positive
162 and 14 negative serum samples and allows direct comparison with other test systems [32]. Both ABCORA

163 versions showed 100% sensitivity and 100% specificity on the verification plasma panel and compared
164 favorably to commercial assay systems (Fig. 1d, Supplementary Table 7). To cross-reference these
165 external verification results, we next compared the sensitivity of the ABCORA tests and three
166 commercial serology test systems on a subset of the SARS-CoV-2 positive training cohort (cohort III,
167 N=171). Assays targeting the N protein (Elecsys® Anti-SARS-CoV-2 (Roche Diagnostics GmbH)), the RBD
168 region of the S protein (Elecsys® Anti-SARS-CoV-2 S assay (Roche Diagnostics GmbH)), and the S1
169 subunit (EUROIMMUN Anti-SARS-CoV-2 ELISA (IgG)) were included. The results confirmed the analysis
170 on the international NIBSC 20/B770 plasma panel, with ABCORA 2.0 and ABCORA 2.3 showing the
171 highest sensitivity amongst the tested assays (Supplementary Table 8).

172 We thus conclude that ABCORA 2.0 seroprofiling in combination with ABCORA 2.3 defines positivity
173 with the highest specificity and sensitivity. The individual antigen response evaluation by ABCORA 2.0
174 defines the stage of seroconversion status based on individual IgM, IgA and IgG cut-off values and
175 thereby complements and maximizes the information that can be obtained by ABCORA 2 seroprofiling.

176

177 **Predicting SARS-CoV-2 neutralization based on ABCORA seroprofiling**

178 Determining neutralization activity is critical to gauge protective immunity. While neutralization can
179 be directly measured with a range of authentic virus or pseudovirus SARS-CoV-2 neutralization tests
180 [5,22,33], applying direct binding or competition tests as surrogate for neutralization activity remains of
181 high interest for diagnostic purposes where cell-based assays are more difficult to implement [33,34]. In
182 particular, S1 and RBD binding and ACE2 competition have been shown to correlate well with
183 neutralization activity [5,8,10,19,33-37]. To explore neutralization predictors based on ABCORA 2.0, we
184 probed in a first step the capacity of ABCORA to derive quantitative S1 and RBD readouts in a subset
185 of SARS-CoV-2 positive patients (N=72). ABCORA 2.0 measurements of serially diluted plasma were
186 conducted to derive 50% effective concentrations (EC50, expressed as reciprocal plasma dilution) and
187 area under the curve values (AUC expressed as MFI) for all 12 SARS-CoV-2 parameters (Fig. 2a, b). In

188 addition, we quantified SARS-CoV-2 RBD and S1 responses via the RBD specific mAb CR3022 [38] (Fig. 2c)
189 and the WHO International Standard Anti-SARS-CoV-2 Immunoglobulin NIBSC 20/136 [32]
190 (Supplementary Fig. 7b, Supplementary Table 9). For this we quantified the respective antibody
191 content of a positive control SARS-CoV-2 donor pool included in all ABCORA measurements and
192 expressed the antibody content of individual plasma samples in relation to it (Fig. 2c, Supplementary
193 Fig. 7). We then probed which of the ABCORA quantitative readouts correlated best with each other,
194 the basic readout of ABCORA 2.0 (MFI-FOE at plasma dilution 1/100), and the quantitative Roche
195 Elecsys S test (U/ml) (Fig. 2c, Supplementary Fig. 7). In addition to the individual antigen parameters,
196 we also considered cumulative response values. These were total spike reactivity (sum of RBD, S1, S2
197 across all Ig classes), Ig class spike reactivity (sum of S1, RBD, S2 for one isotype) and antigen specific
198 reactivity (sum of all Ig classes for one antigen). We observed a genuinely good correlation across the
199 diverse spike parameters tested (Fig. 2d). The notable exception were classical EC50 values, which
200 showed no to weak correlation across all parameters including the commercial test. Interestingly, AUC
201 values, which in contrast to EC50 are a composite measure of concentration and signal strength,
202 performed well. Of note, we observed highly variable SARS-CoV-2 antibody dose response curves,
203 reaching in our cohort individual plateaus over a 4-log range (Supplementary Fig. 7). These plateaus
204 are respected in the AUC readout, and are also recorded by the basic MFI-FOE ABCORA readout at
205 1/100 plasma dilution, but are not considered in EC50 determinations. Indeed the basic MFI-FOE
206 showed a high correlation with the quantitative readouts across the tested variables including the
207 quantitative commercial Roche Elecsys S test.

208 Based on these results, we concluded that the MFI-FOE readout solely at the 1/100 plasma dilution
209 provides a highly reliable estimate for the S1 and RBD antibody content in plasma that can be used as
210 a proxy for quantification without the need to titrate samples. We therefore employed the basic MFI-
211 FOE in a next step to define neutralization predictors.

212 Neutralization activity to Wuhan-Hu-1 in SARS-CoV-2 positive individuals (N=467) using an established
213 SARS-CoV-2 pseudovirus neutralization test [5,22,33] revealed a broad range of 50% neutralizing titers

214 (NT50) (post positive RT-PCR Fig. 3a (N=369), post onset of symptoms, Supplementary Fig. 8a (N=333)),
215 in line with previous findings [5,8]. Early in infection (within 30 days of positive RT-PCR) neutralization
216 titers were significantly higher ($p<0.001$) and correlated better with binding parameters. As expected,
217 IgG responses to spike antigens showed the highest correlation with neutralization activity (Fig. 3b,
218 Supplementary Fig. 8-9). We next grouped patients based on the population into high (NT50 >250,
219 N=332) and no or low neutralizers (NT50 <250, N=135) [39] (Fig. 4a) and compared the prediction ability
220 of six different classification models to assign individuals based on their ABCORA 2.0 binding patterns
221 to these groups. Univariable logistic regression (ULR) models included only one variable: either the
222 mean of MFI-FOE S1 reactivities (ULR-S1), or the mean of MFI-FOE RBD reactivities (ULR-RBD). A
223 multivariable logistic regression (MLR) included both S1 and RBD mean reactivities. The additional
224 models included all 12 antigen reactivities measured in ABCORA and comprised a random forest
225 approach and two MLR strategies based on principle component analysis (PCA, 2 and 4 first axis).
226 Models were compared based on AUC and the BIC (Bayesian information criterion [40]) by cross
227 validation (Fig. 4b, c). All models performed similarly, with the univariable model based on the mean
228 of S1 reactivities (ULR-S1) yielding the best BIC value. Receiver operating curve (ROC) analysis based
229 on ULR-S1 showed a good capacity in predicting neutralization status yielding AUC 0.90 (N=467, Fig.
230 4d). Exploring different cutoffs to balance sensitivity and specificity keeping both above 80%, we chose
231 to assign samples to the high neutralizers group if its predicted probability was above 70%. This
232 corresponds to an 83% specificity in correctly assigning non–neutralizers and 80% sensitivity in
233 assigning neutralizers (Fig. 4d, e). To increase the utility of the ULR-S1 prediction model for clinical
234 diagnostics, we devised a modified neutralization prediction model ULR-S1-SOC based on the SOC
235 values reported for ABCORA 2.0. At 70% predicted probability, ULR-S1-SOC delivers neutralization
236 prediction at similar sensitivity (81%) and specificity (81%) by examining if the composite S1 SOC value
237 (sum of S1 SOC values for IgG, IgA and IgM) is below or above 9.7 (Fig. 4f). Correspondingly, a S1 SOC
238 value above 17.3 corresponds to sensitivity 67% and specificity 94%. Of note, the interrelations
239 between neutralization and S1 levels were equally apparent when we probed a lower cut-off of

240 neutralization (NT50 <100) (Supplementary Fig. 10, Supplementary Table 10). We therefore conclude
241 that the basic SOC readout in ABCORA 2.0 can deliver a reliable prediction of high neutralization
242 activity.
243

244 **Resolution of temporal antibody dynamics by ABCORA seroprofiling**

245 Cross-sectional analysis of antibody reactivity post SARS-CoV-2 diagnosis by RT-PCR (N=369) and post
246 onset of symptoms (N=333) underlined the capacity of ABCORA seroprofiling to dissect onset, peak
247 and waning of SARS-CoV-2 antibody responses (Fig. 5a, b, Supplementary Fig. 11). In individuals with
248 known date of first SARS-CoV-2 RT-PCR diagnosis or onset of symptoms, ABCORA 2.3 detected early
249 seroconversion in 98% (48 of 49) and 100% (9 of 9) of individuals within 7 days post RT-PCR and onset
250 of symptoms, respectively. Besides IgM and IgA reactivity, IgG responses were readily detectable in
251 ABCORA 2.0 after a few days of infection (Supplementary Fig. 11a).

252 Longitudinal assessment of a cohort of convalescent patients up to 11 months post infection (251
253 measurements on 120 patients) highlighted the temporal dynamics of SARS-CoV-2 binding antibodies.
254 We estimated the decay of binding reactivity employing a power law mixed model and identified a
255 significant reduction in RBD, S1, and N in all Ig subtypes (Fig. 5b) with half-lives ranging from 67 to 404
256 days, with IgG N titers decaying the fastest, in line with previous reports [10]. Half-lives of the
257 neutralization relevant IgG responses to RBD and S1 where 125 and 404 days, respectively. Intriguingly,
258 the kinetics of neutralizing antibodies did not mirror the decay rates observed for binding antibodies.
259 Neutralization activity decreased overall at a slower rate, with a half-life of 991 days (Fig 5c). This was
260 in part due to a mixed reactivity pattern with some individuals showing an increase in neutralization
261 activity post positive SARS-CoV-2 RT-PCR [5], while neutralization activity in others rapidly decayed
262 (Supplementary Fig. 11c).
263

264

265 **Effects of HCoV immunity on SARS-CoV-2 acquisition**

266 To enable an investigation of interdependencies between pre-existing immunity to HCoV and SARS-
267 CoV-2 infection, we expanded the ABCORA bead antigen array to include S1 proteins of all four
268 circulating HCoVs (HCoV-NL63, HCoV-229E, HCoV-HKU1, HCoV-OC43) (Supplementary Fig. 12a).
269 According to its capacity to monitor antibodies to five coronaviruses we termed the assay ABCORA 5.0
270 and trained and validated it on the same cohorts as ABCORA 2.0 (Fig. 1). To allow direct comparison
271 with ABCORA 2.0 and use of the neutralization prediction models, we used the threshold-/SOC-based
272 analysis settings of ABCORA 2.0 also for ABCORA 5.0. Based on ABCORA 5.0 measurements of training
273 cohorts I-III, we devised two random forest-based analysis models. ABCORA 5.4 included solely the 12
274 SARS-CoV-2 parameters, ABCORA 5.5 included in addition the S1 HCoV measurements adding up to 24
275 parameters in total. In analogy to ABCORA 2.3, incorporation of HCoV reactivity into the model was
276 advantageous. ABCORA 5.5 provided the highest sensitivity and specificity amongst the analysis
277 algorithms probed ABCORA 5.0 (Supplementary Fig. 12b, Supplementary Table 11).
278 Interdependencies between antibody reactivity to the four HCoVs and SARS-CoV-2 mirrored what we
279 previously observed for HKU1 with a particular high correlation of IgM reactivity of SARS-CoV-2 and
280 HCoVs in pre-pandemic individuals, particularly in those with recent HCoV infection (Supplementary
281 Fig. 13). HCoV infections are frequent but subject to seasonality and prevalence of individual HCoV
282 infections fluctuates [41,42]. In line with this, the prevalence of HCoV responses measured by ABCORA 5.0
283 in local blood donors in January 2019 (N=285), May 2019 (N=288), and January 2020 (N=252) varied
284 considerably (Fig. 6). To enable a time-controlled comparison of HCoV reactivity between SARS-CoV-
285 2-infected and healthy donors, we screened blood donors from May 2020 (N=672), when SARS-CoV-2
286 prevalence was estimated below 2% in Zurich, Switzerland [43], by ABCORA 2.0/5.0 and excluded all
287 samples with SARS-CoV-2 reactivity. The residual May 2020 cohort (N=653) formed a pandemic,
288 healthy donor control group. Interestingly, HCoV reactivity patterns in 2019 and 2020 differed
289 substantially as assessed by one-way ANOVA, with January 2020 showing the comparatively lowest

290 and May 2020 the highest IgA and IgG reactivity, which may indicate a later onset of an HCoV epidemic
291 in 2020 compared to 2019 (t-tests of May 2020 versus other groups shown in Fig. 6).
292 Most intriguingly, a time-matched analysis comparing May 2020 healthy donors with SARS-CoV-2-
293 positive patients sampled in April, May and June 2020 (N=65) revealed significantly lower HCoV
294 reactivity in SARS-CoV-2 positive patients (Fig. 7a). This pattern was also evident when we extended
295 the analysis to include the full cohort of SARS-CoV-2 infected individuals measured with ABCORA 5.0
296 (N=389, sampled from March 2020 to February 2021, Supplementary Fig. 14). Overall, these results
297 indicated that preexisting immune responses to HCoVs may to a certain degree protect against SARS-
298 CoV-2 infection.
299
300
301 **Effects of HCoV immunity in SARS-CoV-2 infection**

302 To explore interdependencies with HCoV immunity further, we next investigated whether HCoV
303 responses are linked to the evolution of SARS-CoV-2 antibodies. To this end, we analyzed antibody
304 responses in plasma of 204 individuals sampled within 60 days post SARS-CoV-2 diagnosis using a linear
305 regression model adjusted for age, gender, time since positive RT-PCR and HCoV reactivity. To stratify
306 HCoV reactivity into high and low HCoV activity, median logMFI-FOE were defined for each HCoV and
307 antibody class. LogMFI-FOE higher than the corresponding median for at least three HCoVs (HKU1,
308 OC43, NL63 or 229E) in a specific Ig class were ranked as having high HCoV activity within this class.
309 First, only reactivities among the same antibody class were explored in the model (i.e. HCoV IgG high
310 on SARS-CoV-2 IgGs). We observed exceptionally strong interdependencies for IgA and IgM responses
311 to SARS-CoV-2, which all were significantly higher in individuals with high HCoV reactivity (Fig. 7b). This
312 strongly suggests that pre-existing HCoV immunity may provide an advantage in mounting SARS-CoV-
313 2 responses. Interdependencies between HCoV IgG and SARS-CoV-2 specific IgG were only observed
314 for the S2 response. Intriguingly, supporting this finding, HCoV S2 helper responses were recently
315 found to boost SARS-CoV-2 immunity, in particular S2 antibody activity [31]. To explore if SARS-CoV-2 IgG

316 may build on recent HCoV IgA and IgM responses we next probed whether HCoV IgM and IgA are linked
317 to elevated SARS-CoV-2 specific IgG levels. While no effect was evident for IgM, we observed a
318 significant association of high HCoV IgA activity on all four measured SARS-CoV-2 responses (Fig. 7c,
319 d). This strongly suggests that recent HCoV infection has a beneficial effect on mounting SARS-CoV-2
320 antibody responses.
321 In a next analysis, we probed if pre-existing HCoV immunity has an impact on disease severity in COVID-
322 19. To this end, we probed HCoV immunity in 80 hospitalized and non-hospitalized individuals infected
323 for less than 30 days (Fig. 8a). Controlling for age and gender, we found that individuals with high pre-
324 existing HCoV reactivity had significantly lower odds to require hospitalization (logistic regression
325 OR=0.16, 95% CI (0.04, 0.67), Fig. 8b, Supplementary Fig. 15). A further stratification of patients by
326 whether they required treatment at an ICU showed a lowered likelihood that patients with high HCoV
327 response rates required hospitalization with intensive care (ordinal regression OR=0.36, 95% CI (0.13,
328 0.96), Fig. 8b, Supplementary Fig. 15). Thus, individuals with high HCoV levels had a 64 % lowered odds
329 of requiring hospitalization according to ordinal rank regression analysis comparing hospitalized in
330 regular wards, in ICU and non- hospitalized individuals (Fig. 8a, b). Collectively, these observations
331 strongly suggest a cross-protective effect of HCoV immunity on shaping the immune defense against
332 SARS-CoV-2.

333

334 **Discussion**

335 Definition of SARS-CoV-2 immunity post vaccination and infection is of immediate importance [44-46].
336 Deciphering antibody correlates of SARS-CoV-2 protection and monitoring vaccine responsiveness are
337 challenging tasks ahead. The magnitude and longevity of protective antibody responses to natural
338 infection and of different vaccines need to be examined to understand parameters that shape
339 protective responses and guide decisions on re-vaccination in non-responders and immunization
340 against novel arising SARS-CoV-2 variants [47]. Likewise, creating means to serologically distinguish

341 between de novo infection, re-infection, and vaccine responses, their durability and failures will remain
342 critical for clinical diagnosis.

343 Here we demonstrate the high utility of multi-parameter seroprofiling in addressing key issues in
344 defining SARS-CoV-2 immunity. Simultaneous detection of antibody responses to a range of SARS-CoV-
345 2 antigens and different Ig classes with ABCORA seroprofiling provided a comprehensive picture of
346 SARS-CoV-2 serologic status in a single examination, which can be useful for clinical diagnosis to
347 determine the presence of reinfection, define reinfection, and respond to vaccination. Computational
348 modeling also allowed predicting plasma neutralization capacity from ABCORA results, enabling a
349 comprehensive assessment of SARS-CoV-2 antibody dynamics and their interplay with HCoV
350 responses. We studied two ABCORA assay versions that both measured HCoV reactivity alongside the
351 12 SARS-CoV-2 parameters. ABCORA 2 included the S1 antigen of HKU1. ABCORA 5 included S1 of all
352 four circulating HCoVs. Notably, computational models that included the HCoV measurements allowed
353 a higher precision in determining SARS-CoV-2 seropositivity, highlighting interdependencies between
354 HCoV and SARS-CoV-2 responses that need to be resolved.

355 Recording reactivity against all four HCoVs in SARS-CoV-2 uninfected and infected individuals we
356 observed intriguing associations. Uninfected individuals displayed higher HCoV reactivity compared to
357 infected individuals suggesting a contribution of HCoV immunity to early defense against SARS-CoV-2.
358 HCoV immunity may also have positive effects in SARS-CoV-2 infection. In agreement with other
359 reports, we noted a cross-feeding of SARS-CoV-2 and HCoV responses in SARS-CoV-2 infection [31,48] with
360 individuals with high HCoV reactivity developing higher SARS-CoV-2 antibody levels. Most notably, pre-
361 existing HCoV immunity had an impact on disease severity in our cohort. SARS-CoV-2 infected
362 individuals with low HCoV reactivity had a higher likelihood of requiring hospitalization.

363 While our study solely measured antibody responses, a potential protective effect of HCoV immunity
364 against SARS-CoV-2 acquisition should not be viewed restricted to antibody activity. Antibodies and
365 cellular immunity may both be relevant and act in concert [31,49-51]. Alternatively, antibody responses

366 measured in the present study may solely document recent HCoV infection and deliver a surrogate
367 measurement of other protective HCoV responses. The link between higher HCoV and SARS-CoV-2
368 reactivity in infected individuals is particularly intriguing. Strongest effects were seen for IgM and IgA
369 HCoV responses, suggesting that recent HCoV immunity provides an early boost to SARS-CoV-2
370 antibody development. Whether this is due to cross-reactive B cell responses on which the SARS-CoV-
371 2 immunity builds on and matures or whether cross-reactive T helper activities play a dominant role
372 as suggested [31] will be important to resolve in forth-coming studies. The exact role and timing of HCoV
373 responses influencing SARS-CoV-2 antibody responses also remain to be defined. Early low-affinity
374 HCoV responses may have a positive impact on the development of SARS-CoV-2 immunity by forming
375 an immune memory on which to build, whereas amplification of non-protective cross-reactive HCoV
376 antibodies according to the antigenic sin principle may have negative effects [30].

377 Although association studies such as ours cannot formally define causality, the implications of our
378 findings are evident: Prior immunity to HCoV may protect to some extent against SARS-CoV-2
379 acquisition, may provide a boost to the development of SARS-CoV-2 specific immunity and with this
380 lower the risk for severe hospitalization. A modest protective effect by HCoV immunity would be a
381 plausible explanation for the high proportion of asymptomatic and mild SARS-CoV-2 infections [52,53].
382 Even more intriguing are future perspectives. As others and we have shown, SARS-CoV-2 and HCoV
383 immunity to infection is often not long-lasting (Fig. 5, Supplementary Fig. 11) [5,54], a limitation that SARS-
384 CoV-2 vaccines hope to overcome. Should SARS-CoV-2 responses in turn provide a degree of defense
385 against HCoV infection, broad protection against coronaviruses may be in reach.

386 **Methods**

387 **Human specimen**

388 Serum and plasma samples collected pre and post emergence of SARS-CoV-2 in Switzerland (pre and
389 post February 2020, respectively) were included. No patient enrollment was conducted for the present
390 study. All experiments involving samples from human donors were conducted with the approval of the
391 responsible local ethics committee (Kantonale Ethikkommission) Zurich, Switzerland (BASEC Nrs 2020-
392 01327, 2020-00363; 2021-00437; 2020-00787), in accordance with the provisions of the Declaration
393 of Helsinki and the Good Clinical Practice guidelines of the International Conference on Harmonisation.
394 Samples were obtained from the following sources: i) Zurich blood donation services (ZHBDS):
395 Anonymized healthy adult plasma from pre-pandemic time points (January 2019, May 2019 and
396 January 2020) and from the first wave of the pandemic in Zurich, Switzerland (May 2020) were
397 provided by the ZHBDS internal serum repository and consent for this study was waived by the ethics
398 committee (BASEC 2021-00437). ii) Anonymized leftover specimens from routine diagnostics at the
399 Institute of Medical Virology, University of Zurich, the University Children Hospital Zurich and the
400 Cantonal Hospital Winterthur (BASEC Nrs 2020-01327, 2021-00437). Written informed consent was
401 obtained from all participants whose sample was taken during the pandemic at the University Hospital
402 Zurich (BASEC 2020-01327). For pandemic samples from other hospitals and pre-pandemic samples
403 consent was waived by the ethics committee. iii) Healthcare workers with RT-PCR confirmed SARS-
404 CoV-2 infection participating in a study at the University Hospital Zurich (BASEC 2020-00363). Written
405 informed consent was obtained from all participants. iv) Male plasma donors participating in a SARS-
406 CoV-2 plasma therapy study conducted at the University Hospital Zurich (CPT-ZHP, Swissmedic
407 2020TpP1004; BASEC 2020-00787). Written informed consent for research was obtained from all
408 participants. The reporting of all human and patient data is in compliance with STROBE statement. Pre-
409 pandemic (SARS-CoV-2 negative, N=825) and confirmed SARS-CoV-2 positive samples (N=389) were
410 divided into training and validation cohorts (Supplementary Table 3). Available demographics data on
411 gender, age, time since positive RT-PCR and symptom onset, and hospitalization status are reported in

412 Supplementary Table 12. The SARS-CoV-2 training cohort (N=175) included plasma collected during
413 infection (N=114) and convalescence (N=61). Per donor only one sampling time point was included,
414 longitudinal samples of donors included in the training cohort were not included in the validation
415 cohort to ascertain independence when assessing the sensitivity and specificity of the different
416 diagnostic methods. The SARS-CoV-2 validation cohort (N=214), comprised plasma collected during
417 infection (N=90, one sampling time point per donor) and convalescence (N=124, 79 convalescent
418 patients with 1-4 longitudinal samples). Multiple time points of convalescent patients were included
419 in the validation data set to capture a wide spectrum of waning antibody titers. Cross-sectional analysis
420 was based on samples with known time since positive RT-PCR (N=369) or known time since symptom
421 onset (N=333), both including the longitudinal analysis observations. Both, time since positive RT-PCR
422 and time since onset were known for 330 samples, with a median time of 3 days between symptom
423 onset and RT-PCR (1st-3rd quartile: 1-7 days). Longitudinal analysis of antibody reactivity was based on
424 251 observations from 120 convalescent patient with known time since positive RT-PCR and time since
425 symptom onset. Neutralization was measured on 467 SARS-CoV-2 RT-PCR positive samples (N=369
426 with known time since positive RT-PCR, N=333 with known time since symptom onset).

427 We further evaluated cross-reactivity ABCORA 2.0 and 5.0 in left-over plasma from routine diagnostics
428 in a pre-pandemic control group with documented, recent HCoV infection (Training II, N=75; OC43
429 (N=27), HKU1 (N=17), NL63 (N=22), 229E (N=9)). Circulating HCoV are commonly only screened for in
430 in hospitalized, severe respiratory infections and immune compromised individuals who routinely
431 undergo a broad screening for respiratory infections. Hence, in this patient group both, reduced
432 antibody reactivity due to immune compromising or elevated HCoV antibody reactivity due to recent
433 or recurring HCoV infection may occur. As this group is diagnostically relevant we considered it prudent
434 to include this cohort as Training II data set to verify if cross-reactivity with SARS-CoV-2 in ABCORA
435 occurs in this setting. Training II data were not included in the threshold definition to not over-
436 represent individuals with severe illness. This HCoV infected group displayed overall lower reactivity
437 with SARS-CoV-2 than plasma from healthy adults but importantly showed no indication of cross-

438 reactivity (Fig. 1a, b). Pandemic samples from anonymous blood donors with unknown SARS-CoV-2
439 status collected in May 2020 (N=672) were not included in training and validation cohorts.

440 **Reagents and cell lines**

441 His-tagged SARS-CoV-2-derived antigens (receptor binding domain (RBD), subunit S1 (S1), subunit S2
442 (S2), nucleocapsid protein (N)) and S1 of the four circulating HCoVs (HKU1, OC43, NL63, 229E) were
443 purchased from Sino Biological Europe GmbH, Eschborn, Germany (Supplementary Table 13). Sources,
444 specifics and concentration of detection and control antibodies and sera used for ABCORA and
445 neutralization tests are listed in Supplementary Table 14. 293-T cells were obtained from the American
446 Type Culture Collection (ATCC CRL-11268) [55]. HT1080/ACE2cl.14 cells [33] were kindly provided by P.
447 Bieniasz, Rockefeller University, NY. Both cell lines were cultured in DMEM containing 10% FCS.

448

449 **Design of multiplex bead assay ABCORA 2.0**

450 We established two bead-based multiplexed SARS-CoV-2 immunoassays (ABCORA 2.0 and ABCORA
451 5.0) that included a range of SARS-CoV-2 and HCoV antigens (Sino Biological Europe GmbH, Eschborn,
452 Germany, Supplementary Table 13). Four SARS-CoV-2 antigens - RBD, S1, S2 and N - were included in
453 both ABCORA 2.0 and ABCORA 5.0. ABCORA 2.0 included in addition S1 of HCoV-HKU1, ABCORA 5.0
454 included S1 of all circulating HCoVs (HCoV-NL63, HCoV-229E, HCoV-HKU1, HCoV-OC43). In brief,
455 individual MagPlex beads (Luminex Corporation, Austin, TX) with unique fluorescent bead regions were
456 chosen for each antigen, beads were coupled and mixtures of antigen-coupled beads incubated with
457 patient plasma in a 96-well plate set-up. Median Fluorescent Intensity (MFI) of bead-bound plasma
458 antibodies were measured utilizing a FlexMap 3D reader (Luminex Corporation, Austin, TX). We
459 designed the assay to fulfil the following criteria: i) high specificity, sensitivity and reproducibility, ii)
460 flexible multiplex design that allows straightforward addition and/or alteration of antigens; iii) wide
461 dynamic range; iv) optional quantification of antibody responses; v) optional recording of antibody
462 responses to HCoVs and vi) use in routine diagnostics and research.

463 We chose a sterically orientation capture via anti-His antibodies to ensure a homogenous antigen
464 display. Therefore, carboxylated MagPlex beads (Luminex Corporation, Austin, TX) were coupled with
465 anti-His antibody (Sino Biological Europe GmbH, Eschborn, Germany, Supplementary Table 14) and
466 then coupled with His-tagged antigens using Bio-Plex Amine coupling (Bio-Rad Laboratories AG,
467 Cressier, Switzerland) according to the manufacturer's instructions and as described [56].

468 Serum/plasma titration is in general considered the most accurate strategy to retrieve quantitative
469 information on antibody reactivity. However, in diagnostic use tests ideally should deliver (semi)-
470 quantitative information from a single serum dilution to permit a sufficient throughput. The finalized
471 assay conditions covered a 2-log MFI range across all probed antigen-Ig combinations (Supplementary
472 Fig. 1). Ratifying the validity of using a single plasma dilution, we confirmed that plasma from SARS-
473 CoV-2 positive patients and pre-pandemic SARS-CoV-2 negative plasma samples show optimal dose
474 response curves over a wide plasma dilution range (Supplementary Fig. 1f). Importantly, a 1/100
475 dilution of plasma was in all cases close to the maximum signal, underlining that increasing plasma
476 concentration would not increase signal intensity but rather endanger decreasing signals due to
477 prozone effects (Supplementary Fig. 1f).
478 Maximal anti-His antibody loading was achieved at 5 µg antibody per million beads (Supplementary
479 Fig. 1c) and used as standard coupling condition. In the final protocol, five million anti-His antibody
480 coupled magnetic beads were incubated with His-tagged antigens diluted in PBS at a concentration of
481 320 nM. Phycoerythrin (PE)-labeled secondary antibodies specific to IgG, IgA or IgM were used as
482 detector antibodies (Supplementary Table 14). Quality control of the antigen loading was performed
483 by incubating the beads with monoclonal antibodies targeting the corresponding CoV-derived antigen
484 as detailed in Supplementary Table 13. Analysis was performed with the FlexMap 3D reader (Luminex
485 Corporation, Austin, TX) with the acquisition of at least of 50 beads per bead region. Results are
486 recorded as MFI per bead region.

487 Several control measures were installed to ascertain inter- and intra-assay performance. To ascertain
488 a low assay-to-assay variability, large batches of individual antigen-loaded beads were prepared and

489 frozen in aliquots until use at -20°C to circumvent decay of the antigen-coupled beads (Supplementary
490 Fig. 1). Individual coupled beads were mixed on the test day to yield the required antigen bead cocktail.
491 Cocktails contained 60 beads per bead region per µl. In addition to the SARS-CoV-2 and HCoV bead
492 regions, each cocktail included an empty bead region (no antigen coupled) to control for unspecific
493 binding. Quality control and validation procedures for the FlexMap 3D instrument were done on each
494 day of experiment according to manufacturer's instructions. The variability of the assay was analyzed
495 as follows [56] : plasma samples from 20 RT-PCR confirmed SARS-CoV-2 infected patients were pooled
496 and tested over a range of seven dilutions in 31 different titrations performed on 10 different days
497 (Supplementary Fig. 2). Across all antigens and Ig classes, signals were retained over the test period of
498 25 days post bead coupling. Coefficients of variation (CV) of the binding signal across titrations of the
499 12 antigen-Ig class combinations proved low (range: 0.010-0.128, median 0.059, Supplementary Fig.
500 3c, d, Supplementary Tables 1, 2). Same-day and day-to day variability proved low and comparable
501 (Supplementary Fig. 3e, f). Below a 1/100 plasma concentration, CV increased markedly
502 (Supplementary Fig. 3d), defining 1/100 as highest concentration (lowest plasma dilution) to be tested
503 in the assay. A 1/100 plasma dilution was thus defined as the basic dilution for screening plasma in
504 ABCORA 2.0 when a qualitative (i.e. presence or absence of SARS-CoV-2 specific antibodies) or semi-
505 quantitative (i.e. MFI signal intensity) readout is required.

506 All ABCORA measurements were derived from single measurements unless stated otherwise. To
507 measure SARS-CoV-2 specific antibodies in patient plasma, heat inactivated plasma (1 h at 56°C) was
508 diluted 1/100 in PBS-BSA 1% unless otherwise stated. 50 µl diluted plasma were incubated with 50 µl
509 of the ABCORA antigen bead cocktail for 30 minutes at room temperature in 96-well plates, washed
510 three times with PBS-BSA 1% and incubated in separate reactions with phycoerythrin (PE)-labeled
511 detector antibodies for IgG, IgA or IgM at a final concentration of 1/500 in PBS-BSA 1%. This dilution
512 was previously defined by titration of the detector antibodies to yield optimal MFI signals. After 45
513 minutes of incubation at room temperature, beads were washed three times with PBS-BSA 1% and

514 analyzed in 96-well plates on the FlexMap 3D reader (Luminex Corporation, Austin, TX). A minimum of
515 50 bead reads per antigen was acquired.

516 To control for genuine cross-reactive antibodies, each plasma sample was assessed with beads without
517 antigen (empty bead control) in combination which each detector antibody. For analysis, raw MFI
518 values were transformed to MFI-FOE to correct for background binding. We established mean empty
519 bead MFI-FOE for IgG, IgA and IgM of pre-pandemic healthy donors (N=1016) and set the mean MFI-
520 FOE + 4x standard deviation as threshold for the empty bead control. In absolute levels, these
521 thresholds amounted to MFI-FOE 41.58 (IgG), 55.91 (IgA) and 269.47 (IgM). Measurements for which
522 the empty bead control recorded values above this threshold were considered invalid and repeated.
523 Each Luminex analysis 96-well plate was set up to contain the same set of control samples, namely 7
524 serial 4-fold dilutions of a SARS-CoV-2 positive control donor pool (N=20 donors, starting dilution
525 1/100, Supplementary Fig. 1f) and a pre-pandemic healthy donor pool (dilution 1/100, N=20 donors,
526 Supplementary Fig. 1f). These positive and negative controls allow to control assay performance across
527 independent measurements and in addition enable retrospective standardization against external
528 controls if needed.
529

530 **Definition of SARS-CoV-2 seropositivity in ABCORA 2.0 and ABCORA 5.0**

531 To distinguish SARS-CoV-2-specific from cross-reactive antibodies, we defined MFI-FOE thresholds for
532 each of the 12 SARS-CoV-2 antigen and Ig class combinations based on plasma antibody reactivity in
533 training cohorts (Supplementary Table 3 and 4). These included pre-pandemic healthy donor plasma
534 (Training I, N=573), donors with recent HCoV infection (Training II, N=75; OC43 (N=27), HKU1 (N=17),
535 NL63 (N=22), 229E (N=9)) and donors with confirmed SARS-CoV-2 infection (Training III, N=175).
536 Thresholds were set to minimize false-positives while ensuring sensitivity for SARS-CoV-2 antibody
537 detection and to reach an overall specificity above 99% and included levels for border-line reactivity
538 for IgG RBD, IgG S1 and IgG N to allow also modest antibody reactivity to these antigens to be

539 examined. MFI-FOE reads of individual samples were transformed into signal-over cut-off (SOC) values
540 (MFI-FOE/threshold). SOC values are used for assessing positive reactivity for each individual antigen-
541 antibody class combination, with SOC >1 denoting positive reactivity, SOC <1 denoting negative
542 reactivity. When setting individual thresholds, it must be considered that for each of the 12 probed
543 activities cross-reactivities may occur. With 12 individual SOC parameters recorded, overall specificity
544 will decrease if any positive SOC independently suffices to rate a sample overall as SARS-CoV-2
545 antibody positive. To exemplify: Assuming independent responses, even a high 99% specificity for each
546 antigen will add up to an overall low 88% specificity across the entire assay. We thus required for SARS-
547 CoV-2 positive calling in ABCORA 2.0 a minimum of two specificities to reach activity above threshold.
548 The combined SOC values used to define the overall serostatus of a given sample are detailed in
549 Supplementary Table 5. For IgG RBD, S1 and N, for which we also recorded border-line SOC activity,
550 we allowed for a combination of 1 antigen reactivity SOC >1, the second reactivity SOC > border line.
551 The final threshold and positive call criteria allowed for a differentiation of partial (partial (early
552 seroconversion with only IgM and IgA responses) to full seroconversion (including IgG responses)
553 (Supplementary Table 5). In addition, the criteria denote samples with weak reactivity and/or
554 indeterminate reactivity (Supplementary Table 5).

555 To ease comparison between ABCORA 2.0 and ABCORA 5.0 the same threshold cut-offs were used for
556 ABCORA 5.0. We chose not to create specific cut-off thresholds for HCoV antibody reactivity as an
557 accurate definition of a negative response is complex due to the wide-spread exposure to HCoVs and
558 considerable antibody cross-reactivity between them. HCoV responses were however included in the
559 statistical analyses as MFI-FOE values.

560

561 **Definition of SARS-CoV-2 seropositivity using logistic regression classification**

562 Classification of seropositive versus seronegative samples in ABCORA 2.1 was realized using logistic
563 regression. The identical training and validation data used for the establishment for ABCORA 2.0 were

564 used. As the ABCORA 2.0 binding reactivities were highly correlated, we included the following
565 variables in the model (Supplementary Fig. 6a): the mean value of all IgG MFI-FOE responses (RBD, S1,
566 S2, N), the mean value of the IgA MFI-FOE responses against RBD, S1 and S2, and the mean value of
567 the IgM MFI FOE responses against RBD, S1 and S2. IgA and IgM responses to N were excluded as they
568 were not clustering with the other responses of the same Ig class (Supplementary Fig. 6a). The logistic
569 regression was used to estimate and predict the probability of a given sample to be positive (p) as
570 described in equation (1).

571 (1) $$p = \frac{\exp(\beta 0+\beta G*mean(IgG{:}RBD,S1,S2,N)+\beta A*mean(IgA{:}RBD,S1,S2)+\beta M*mean(IgM{:}RBD,S1,S2))}{1+\exp(\beta 0+\beta G*mean(IgG{:}RBD,S1,S2,N)+\beta A*mean(IgA{:}RBD,S1,S2)+\beta M*mean(IgM{:}RBD,S1,S2))}$$

572 Parameters $\beta 0$, βG, βA and βM were estimed on the training dataset. A sample was then defined as
573 positive if its predicted probability of being positive was above a threshold c'. This threshold was
574 defined as to obtain a specificity of at least 0.99 and maximal sensitivity on the training dataset
575 (similarly to c for the random forest). In summary, in ABCORA 2.1, any new sample is defined as
576 seropositive if its probability of being seropositive as estimated by the logistic regression is above c'.
577 Analyses were performed in R version 3.6.3.

578

579 **Definition of SARS-CoV-2 seropositivity using random forest classification**

580 Classification of seropositive versus seronegative samples in context of ABCORA 2.0 and ABCORA 5.0
581 was realized using a random forest approach following the basic setup of random forests as described
582 in [57]. The random forest itself was built of an ensemble of 1000 classification trees using MFI-FOE
583 responses (IgA, IgG and IgM against RBD, S1, S2, N). The probability of a sample being positive as
584 predicted by the random forest is the average of the probabilities over all 1000 trees. Finally, a sample
585 is defined as positive if its probability of being positive is above a threshold c, which is defined as to
586 obtain a specificity of at least 0.99 and a maximal sensitivity on the training dataset. In summary, any
587 new sample is defined as seropositive if its probability of being seropositive as estimated by the
588 random forest is above the threshold c. We conducted a series of random forest analyses that

589 considered either only SARS-CoV-2 responses or SARS-CoV-2 and HCoV responses in ABCORA 2.0 and
590 ABCORA 5.0: ABCORA 2.2 and ABCORA 2.3 were trained and used for prediction on ABCORA 2.0 data
591 and included only SARS-CoV-2 responses or SARS-CoV-2 and HKU1 responses, respectively. ABCORA
592 5.4 (SARS-CoV-2 responses only) and ABCORA 5.5 (SARS-CoV-2 and HCoV responses) were trained on
593 ABCORA 5.0 data. Details on the data inclusion for the respective models are listed in Supplementary
594 Table 3 and Supplementary Table 11. Analyses were performed in R version 3.6.3 using packages
595 random Forest and ranger [58-61].

596 To ensure robustness of our findings, we performed a sensitivity analysis by randomizing the training
597 and validation datasets using a 5-fold cross validation method. Both sets of positives and negatives
598 samples were divided in 5 equal parts and we defined that way 5 validation sets (consisting of the i-th
599 set of positives and the i-th set of negatives, i=1.5). The rest of the data was used for training the
600 ABCORA 2.3 random forest. For each validation set, the specificity and sensitivity of the random forest
601 were computed on the training, validation and training+validation sets (Supplementary Table 6).

602

603 **Validation and verification using external controls**

604 We used the Anti-SARS-CoV-2 Verification Panel for Serology Assays (NIBSC code: 20/B770, NIBSC) to
605 verify the performance of the ABCORA 2.0 and ABCORA 2.3 test. Serum samples of the verification
606 panel measured by ABCORA 2.0/2.3 as described and results compared with the results of
607 commercially available assays reported by the NIBSC ([32] and Supplementary Table 7). We further
608 verified the sensitivity of the ABCORA 2 test in detecting SARS-CoV-2 infection in a direct comparison
609 with commercial tests. Antibody status of plasma from SARS-CoV-2 positive individuals (N=171) were
610 analyzed with the following test systems: Included test systems targeted the N protein (Elecsys® Anti-
611 SARS-CoV-2 (Roche Diagnostics GmbH)), the RBD region of the S protein (Elecsys® Anti-SARS-CoV-2 S
612 assay (Roche Diagnostics GmbH)), and the S1 subunit (EUROIMMUN Anti-SARS-CoV-2 ELISA (IgG))

613 (Supplementary Table 8). All assays were performed according to the manufacturer's instructions in
614 the diagnostics unit of the Institute of Medical Virology, University of Zurich, Switzerland.

615

616 **SARS-CoV-2 binding antibody titers**

617 To define binding antibody titers, 8 serial 4-fold dilutions starting with a 1/25 dilution of plasma were
618 prepared and measured in ABCORA 2.0. To derive quantitative information, MFI values were corrected
619 for background activity (MFI-empty bead control) and we defined the area under the MFI curve (AUC)
620 across the dilution series for each antigen-Ig combination. As a second quantitative readout, we
621 calculated 50% effective titer concentrations (EC50) using a four-parameter logistic curve
622 (y=Bottom+(Top-Bottom)/(1+10^((logEC50-X)*HillSlope).

623

624 **Quantification of SARS-CoV-2 S1 and RBD activity**

625 We used two approaches to standardize SARS-CoV-2 S1 and RBD activity. The first was based on the
626 S1/RBD specific antibody CR3022 ([38] and Supplementary Table 14). Serial dilutions of IgG, IgA and IgM
627 versions of CR3022 were used to create standard curves on RBD and S1 coated beads. The linear range
628 of the standard and sample dilution curve was used for quantitation. We fitted a four-parameter
629 logistic curve (y=Bottom+(Top-Bottom)/(1+10^((logEC50-X)*HillSlope) (Supplementary Fig. 7b)
630 through which MFI values of measured samples are interpolated into a corresponding concentration
631 of antibody (µg/ml). We used this approach to quantify the concentration of RBD and S1 antibody
632 reactivity in the positive donor control, and used titrations of the donor pool included on each ABCORA
633 plate to calculate the S1 and RBD content of plasma samples in relation to it. We used the same
634 strategy in combination with the WHO International Standard Anti-SARS-CoV-2 Immunoglobulin
635 (NIBSC 20/136 [32]) to defer IU/ml content of the internal ABCORA positive donor pool and the individual
636 specimen tested (Supplementary Fig. 7). The WHO International Standard consists of a pool of plasma
637 from individuals with confirmed SARS-CoV-2 infection. RBD and S1 content of the ABCORA positive

638 donor pool quantified via the polyclonal WHO standard was highly similar within each Ig class
639 (Supplementary Fig. 7b). In contrast, RBD values estimated by the mAb CR3022 were a factor 2.4 – 3.9
640 lower than the corresponding S1 values, suggesting an affinity difference of CR3022 for the two
641 antigens (Supplementary Fig. 7b).

642

643 **Temporal evolution of SARS-CoV-2 binding antibody response**

644 Antibody binding of 140 convalescent patients was measured longitudinally in 274 measurements with
645 ABCORA 2.0, including 251 measurements from 120 patients with known time since positive RT-PCR.
646 We assumed the antibodies (analyzed as logMFI-FOE) were declining with time from 21 days after
647 positive RT-PCR and estimated the decay using a power law mixed model with random effect on the
648 intercept [62]. As time measures days post first positive RT-PCR result (Fig. 5b) or days post onset of
649 symptoms (Supplementary Fig. 11b) were employed. Half-lives (t1/2, in days) of significant response
650 with negative decays were calculated based on the respective estimated decay parameters. Analyses
651 were performed in R version 3.6.3 using packages lme4 and lmerTest [63].

652

653 **SARS-CoV-2 pseudo-neutralization assay**

654 SARS-CoV-2 plasma neutralization activity was defined using an HIV-based pseudovirus system as
655 described [33]. The env-inactivated HIV-1 reporter construct pHIV-1NL4-3 ΔEnv-NanoLuc (pHIV-
656 1Nanoluc) and HT1080/ACE2cl.14 cells were kindly provided by P. Bieniasz, Rockefeller University, NY,
657 USA. To create a SARS-CoV-2 spike expression plasmid (P_CoV2_Wuhan), a codon-optimized C
658 terminal truncated (AA 1255-1273) spike encoding gene of strain Wuhan-Hu-1 (GenBank accession no.
659 MN908947, [https://www.ncbi.nlm.nih.gov/nuccore/MN908947]) was synthesized (GeneArt, Thermo
660 Fisher Scientific, Waltham, MA) and cloned into pcDNA.3.1. Pseudotyped SARS-CoV-2 spike expressing
661 viruses were generated by co-transfecting 293-T cells with a mixture of pHIV-1Nanoluc,
662 P_CoV2_Wuhan and PEI Max (Polysciences Europe GmbH, Hirschberg, Germany). After 48h virus

663 supernatants were filtered (0.2 µm) and stored in aliquots at -80°C until use. Infectivity of virus stocks
664 was measured by infection of HT1080/ACE2cl.14 cells. For this 384-well culture plate pre-treated with
665 poly-L-Lysine were seeded with HT1080/ACE2cl.14 (2200 cells/well) one day before the assay. Cells
666 were infected with titrated virus stocks and NanoLuc luciferase activity in cell lysates measured 48 h
667 post infection using the Nano-Glo Luciferase Assay System (Promega, Fitchburg, WI). For this, cells
668 were washed once with PBS, supernatant was removed and cells were lysed with 20 µl/well of
669 Luciferase Cell Lysis reagent (Promega, Fitchburg, WI) for 15 min under continuous shaking at room
670 temperature. 20 µl of 1/ 50 diluted NanoGlo buffer were added and NanoLuc luciferase activity
671 (relative light units, RLU) was measured after 5 min incubation at room temperature on a Perkin Elmer
672 EnVision reader. Input of SARS-CoV-2 pseudoviruses for neutralization assays was adjusted to yield
673 virus infectivity corresponding to 5-10 x10^6 RLU (corresponding to 100-250-fold over background RLU
674 values) in the absence of inhibitors. To measure plasma neutralization activity six serial 4-fold dilutions
675 of plasma starting at a 1/25 dilution were prepared. 20 µl of the diluted plasma and 20 µl of virus were
676 pre-incubated for 1 h at 37°C and then 30 µl of the virus/plasma mix were transferred to 384-well
677 plates seeded with HT1080/ACE2cl.14 cells in a volume of 30 µl. This resulted in a final concentration
678 of the plasma starting dilution of 1/100. Plasma neutralization titers causing 50%, 80% and 90%
679 reduction in viral infectivity (NT50, NT80 and NT90, respectively) compared to controls without plasma
680 were calculated by fitting a sigmoid dose–response curve (variable slope) to the RLU data, using
681 GraphPad Prism with constraints (bottom=0, top=100). If 50% inhibition was not achieved at the lowest
682 plasma dilution of 1/100, a 'less than' value was recorded. All measurements were conducted in
683 duplicates.

684

685 **Predicting neutralization based on ABCORA binding activity**

686 To compare the ability of SARS-CoV-2 binding activity measured in ABCORA 2.0 to predict the
687 neutralization status, we measured neutralization activity to Wuhan-Hu-1 in SARS-CoV-2 positive

688 individuals (N=467) and classified individuals as high neutralizers (NT50 >250, N=332) and low
689 neutralizers (NT50 <250, N=135). Six different classification models were designed to assign individuals
690 to the high or low neutralizers category, based on their ABCORA2.0 binding patterns we established
691 two univariable logistic regression (ULR) models that included mean MFI-FOE spike antigen S1
692 reactivities and mean MFI-FOE spike antigen RBD reactivities, respectively. S1 and RBD were chosen
693 due to their highest correlation with NT50 (r=0.82 and r=0.80 for the total spike reactivities of S1 and
694 RBD respectively, Supplementary Fig. 9). In addition to these two ULR, we established a multivariate
695 logistic regression model including both mean S1 and RBD reactivities (MFI). We further devised three
696 models that considered all 12 SARS-CoV-2 binding parameters recorded by ABCORA 2.0. Two
697 multivariable logistic regression models were based on a principal component analysis on all binding
698 activities and included the first two (respectively four) principal components, which explained 60%
699 (respectively 75%) of the variance in the data. We also included in our model comparison a
700 classification based on a random forest analysis that incorporated all 12 SARS-CoV-2 binding activity
701 variables.

702 For all 6 models, performance was assessed in 100 cross-validation sets: each set was built by randomly
703 sampling without replacement among the 467 measurements available. 80% of the data set was used
704 to train the model (N=374). Prediction of neutralization status was realized on the other 20% (N=93)
705 and compared to the true NT50 value and neutralization status, using a roc curve. The area under the
706 curve (AUC) was computed for all 6 models in each cross-validation run. The Bayesian information
707 criterion (BIC) was computed for all 5 logistic regressions in each cross-validation run.

708 To increase the utility of the ULR-S1 prediction model for clinical diagnostics we devised a modified
709 neutralization prediction model ULR-S1-SOC based on the signal over cut-off (SOC) values reported for
710 ABCORA 2.0. The ULR-S1-SOC estimates the probability of NT50 >250 based on the sum of S1 SOC
711 values for IgG, IgA and IgM as indicated in equation (2).
712

713 $$(2)\ P(NT50 > 250) = \frac{\exp(a + b * log10(sum\ S1\ SOC))}{1 + \exp(a + b * log10(sum\ S1\ SOC))}$$

714

715 With estimated values: a= -2.6447 and b= 3.5353.

716 ULR-S1-SOC estimates for the probability of NT50 >100 were analyzed in analogy (Supplementary Table
717 10 and Supplementary Fig. 10).

718

719 **Association between HCoVs and SARS-CoV-2 reactivities**

720 To explore the association between HCoVs and SARS-CoV-2 reactivities, we defined a new HCoV
721 response variable (HCoV high/low) for each antibody class (IgG, IgA, IgM) as follows: a patient had high
722 HCoV Ig reactivity for a given antibody class if its measurements were higher than the population
723 median in at least three out of the four HCoV measurements (HKU1, OC43, NL63, 229E). To assess
724 interdependencies between HCoV and SARS-CoV-2 responses, we then included the HCoV response
725 variable in a linear regression model of SARS-CoV-2 reactivities in the same antibody class. The linear
726 regression models were estimated on a subset of SARS-CoV-2 positive patients (N=204), measured on
727 ABCORA 5.0 less than 60 days since positive RT-PCR. The restriction to 60 days was chosen to allow
728 modeling the effect of time with splines. This time period restriction further guaranteed a gender
729 balance, as convalescent donors with longer follow up were all males recruited for a plasma therapy
730 study (CPT-ZHP, Swissmedic 2020TpP1004). Regression analyses were adjusted on time (days post
731 positive RT-PCR or onset of symptoms; as a spline with 3 degrees of freedom), age (as a spline with 3
732 degrees of freedom) and gender.

733 Among the 204 patients analyzed for interdependencies, information regarding hospitalization status
734 (not hospitalized, hospitalized not in ICU, hospitalized in ICU) was known for 160 of them. For 80
735 patients we had samples that were collected less than 30 days since SARS-CoV-2 diagnosis by positive
736 RT-PCR allowing an estimate of HCoV levels close to SARS-CoV-2 acquisition. We performed an
737 additional analysis on this subset of patients using an ordinal regression and a logistic regression to

predict the hospitalization status depending on high or low IgG HCoV reactivity, adjusted on age (as a spline with 3 degrees of freedom) and gender. We checked for robustness of the result in a sensitivity analysis by adjusting on time since positive RT-PCR in addition to age and gender (Supplementary Fig. 15).

Statistical analysis

Statistical analyses were performed in R (Version 3.6.3). Figures were made using the ggplot2 package [64]. When included, boxplots represent the following: median with the middle line, upper and lower quartiles with the box limits, 1.5x interquartile ranges with the whiskers and outliers with points. Heatmaps were made using the ComplexHeatmap package [65]. Significance of Spearman rank correlations were assessed through asymptotic t approximation. Differences in means between two groups with independent measures were tested using two-sided t-tests. When applicable, multiple testing was adjusted using Bonferroni correction for multiple comparisons. A one-way ANOVA with 3 degrees of freedom was used in addition to two-tailed t-tests in Fig. 6 to provide insights on overall versus group comparison. When analyzing datasets including repeated measurements of the same individuals (Fig. 3a, Fig. 5b, Fig. 5c, Supplementary Fig. 8a, Supplementary Fig. 11b), we used linear and power-law mixed models with time since positive RT-PCR or time since symptom onset (continuous or binary variable) as fixed effect and individual as random effect. In the case of Fig. 5c and Supplementary Fig. 11c, the decreasing slope of neutralization titers was estimated by considering only individuals with neutralization titers above the detection levels (NT50 >100) at their first measurement. For all linear mixed models, a Satterthwaite approximation for a two-sided t-test was used to determine if the estimated slope was significantly different from 0. In addition, half-lives were obtained from the decay rate estimated on the log of either MFI-FOEs (Fig. 5b, Supplementary Fig. 11b) or NT50s (Fig. 5c, Supplementary Fig. 11c) as follows: t1/2=t0*exp(log10(2)/rate), with t0=21 days since positive RT-PCR or since symptom onset. In Fig. 7b and 7c, linear regressions were used to estimate the association

763 between HCoV and SARS-CoV-2 reactivities: a Student t-test with two-sided hypothesis was used to
764 assess if this association was significantly different from 0.
765

766 **Data availability**

767 The raw serological measurements generated in this study are provided in Supplementary Table 15.
768 Data depicted in charts and graphs are made available in the Source Data file.

769

770 **Code availability**

771 Codes to assess serostatus based on the ABCORA 2.3 method are available at:
772 https://github.com/chlpasin/SARS-CoV-2-serology [66].

773 **References**

774 1 Rydyznski Moderbacher, C. *et al.* Antigen-Specific Adaptive Immunity to SARS-CoV-2 in Acute
775 COVID-19 and Associations with Age and Disease Severity. *Cell* **183**, 996-1012 e1019,
776 doi:10.1016/j.cell.2020.09.038 (2020).
777 2 Wheatley, A. K. *et al.* Evolution of immune responses to SARS-CoV-2 in mild-moderate
778 COVID-19. *Nature Communications* **12**, 1162, doi:10.1038/s41467-021-21444-5 (2021).
779 3 Wang, Z. *et al.* Enhanced SARS-CoV-2 neutralization by dimeric IgA. *Sci Transl Med* **13**,
780 doi:10.1126/scitranslmed.abf1555 (2021).
781 4 Robbiani, D. F. *et al.* Convergent antibody responses to SARS-CoV-2 in convalescent
782 individuals. *Nature* **584**, 437-442, doi:10.1038/s41586-020-2456-9 (2020).
783 5 Gaebler, C. *et al.* Evolution of antibody immunity to SARS-CoV-2. *Nature*,
784 doi:10.1038/s41586-021-03207-w (2021).
785 6 Muecksch, F. *et al.* Longitudinal analysis of serology and neutralizing antibody levels in
786 COVID19 convalescents. *J Infect Dis*, doi:10.1093/infdis/jiaa659 (2020).
787 7 Long, Q.-X. *et al.* Clinical and immunological assessment of asymptomatic SARS-CoV-2
788 infections. *Nature Medicine* **26**, 1200-1204, doi:10.1038/s41591-020-0965-6 (2020).
789 8 Robbiani, D. F. *et al.* Convergent antibody responses to SARS-CoV-2 in convalescent
790 individuals. *Nature* **584**, 437-442, doi:10.1038/s41586-020-2456-9 (2020).
791 9 Aziz, N. A. *et al.* Seroprevalence and correlates of SARS-CoV-2 neutralizing antibodies from a
792 population-based study in Bonn, Germany. *Nat Commun* **12**, 2117, doi:10.1038/s41467-021-
793 22351-5 (2021).
794 10 Fenwick, C. *et al.* Changes in SARS-CoV-2 Spike versus Nucleoprotein Antibody Responses
795 Impact the Estimates of Infections in Population-Based Seroprevalence Studies. *J Virol* **95**,
796 doi:10.1128/JVI.01828-20 (2021).
797 11 Buss, L. F. *et al.* Three-quarters attack rate of SARS-CoV-2 in the Brazilian Amazon during a
798 largely unmitigated epidemic. *Science* **371**, 288-292, doi:10.1126/science.abe9728 (2021).
799 12 Diagnostics, E. R. <https://diagnostics.roche.com/global/en/products/params/elecsys-anti-
800 sars-cov-2.html> (
801 13 Abbott. <https://www.corelaboratory.abbott/us/en/offerings/segments/infectious-
802 disease/sars-cov-2> (
803 14 Euroimmun. <https://www.euroimmun.com/products/infection-diagnostics/id/sars-cov-2-
804 infection-covid-19/> (
805 15 Pinto, D. *et al.* Cross-neutralization of SARS-CoV-2 by a human monoclonal SARS-CoV
806 antibody. *Nature* **583**, 290-295, doi:10.1038/s41586-020-2349-y (2020).
807 16 Piccoli, L. *et al.* Mapping Neutralizing and Immunodominant Sites on the SARS-CoV-2 Spike
808 Receptor-Binding Domain by Structure-Guided High-Resolution Serology. *Cell* **183**, 1024-
809 1042.e1021, doi:https://doi.org/10.1016/j.cell.2020.09.037 (2020).
810 17 Thomson, E. C. *et al.* Circulating SARS-CoV-2 spike N439K variants maintain fitness while
811 evading antibody-mediated immunity. *Cell* **184**, 1171-1187 e1120,
812 doi:10.1016/j.cell.2021.01.037 (2021).
813 18 Müller, L. *et al.* Sensitivity of anti-SARS-CoV-2 serological assays in a high-prevalence setting.
814 *European Journal of Clinical Microbiology & Infectious Diseases*, doi:10.1007/s10096-021-
815 04169-7 (2021).
816 19 Rogers, T. F. *et al.* Isolation of potent SARS-CoV-2 neutralizing antibodies and protection from
817 disease in a small animal model. *Science* **369**, 956-963, doi:10.1126/science.abc7520 (2020).
818 20 Barnes, C. O. *et al.* Structures of Human Antibodies Bound to SARS-CoV-2 Spike Reveal
819 Common Epitopes and Recurrent Features of Antibodies. *Cell* **182**, 828-842 e816,
820 doi:10.1016/j.cell.2020.06.025 (2020).
821 21 Starr, T. N. *et al.* Deep Mutational Scanning of SARS-CoV-2 Receptor Binding Domain Reveals
822 Constraints on Folding and ACE2 Binding. *Cell* **182**, 1295-1310 e1220,
823 doi:10.1016/j.cell.2020.08.012 (2020).

22 Weisblum, Y. *et al.* Escape from neutralizing antibodies by SARS-CoV-2 spike protein variants. *Elife* **9**, doi:10.7554/eLife.61312 (2020).
23 Zhang, S. F. *et al.* Epidemiology characteristics of human coronaviruses in patients with respiratory infection symptoms and phylogenetic analysis of HCoV-OC43 during 2010-2015 in Guangzhou. *PLoS One* **13**, e0191789, doi:10.1371/journal.pone.0191789 (2018).
24 van der Hoek, L. *et al.* Burden of disease due to human coronavirus NL63 infections and periodicity of infection. *Journal of Clinical Virology* **48**, 104-108, doi:https://doi.org/10.1016/j.jcv.2010.02.023 (2010).
25 Huang, A. T. *et al.* A systematic review of antibody mediated immunity to coronaviruses: kinetics, correlates of protection, and association with severity. *Nat Commun* **11**, 4704, doi:10.1038/s41467-020-18450-4 (2020).
26 Amanat, F. *et al.* A serological assay to detect SARS-CoV-2 seroconversion in humans. *Nat Med* **26**, 1033-1036, doi:10.1038/s41591-020-0913-5 (2020).
27 Ladner, J. T. *et al.* Epitope-resolved profiling of the SARS-CoV-2 antibody response identifies cross-reactivity with endemic human coronaviruses. *Cell Rep Med* **2**, 100189, doi:10.1016/j.xcrm.2020.100189 (2021).
28 *Diagnostic testing for SARS-CoV-2- Interim guidance*, <https://www.who.int/publications/i/item/diagnostic-testing-for-sars-cov-2> (
29 Ng, K. W. *et al.* Preexisting and de novo humoral immunity to SARS-CoV-2 in humans. *Science* **370**, 1339-1343, doi:10.1126/science.abe1107 (2020).
30 Francis, T. On the Doctrine of Original Antigenic Sin. *Proceedings of the American Philosophical Society* **104**, 572-578 (1960).
31 Loyal, L. *et al.* Cross-reactive CD4(+) T cells enhance SARS-CoV-2 immune responses upon infection and vaccination. *Science*, doi:10.1126/science.abh1823 (2021).
32 NIBSC.org. <https://www.nibsc.org/products/brm_product_catalogue/detail_page.aspx?catid=20/136> (
33 Schmidt, F. *et al.* Measuring SARS-CoV-2 neutralizing antibody activity using pseudotyped and chimeric viruses. *bioRxiv*, doi:10.1101/2020.06.08.140871 (2020).
34 Pinto, D. *et al.* Cross-neutralization of SARS-CoV-2 by a human monoclonal SARS-CoV antibody. *Nature* **583**, 290-295, doi:10.1038/s41586-020-2349-y (2020).
35 Brouwer, P. J. M. *et al.* Potent neutralizing antibodies from COVID-19 patients define multiple targets of vulnerability. *Science* **369**, 643-650, doi:10.1126/science.abc5902 (2020).
36 Wu, Y. *et al.* A noncompeting pair of human neutralizing antibodies block COVID-19 virus binding to its receptor ACE2. *Science* **368**, 1274-1278, doi:10.1126/science.abc2241 (2020).
37 Chi, X. *et al.* A neutralizing human antibody binds to the N-terminal domain of the Spike protein of SARS-CoV-2. *Science* **369**, 650-655, doi:10.1126/science.abc6952 (2020).
38 Yuan, M. *et al.* A highly conserved cryptic epitope in the receptor binding domains of SARS-CoV-2 and SARS-CoV. *Science* **368**, 630-633, doi:10.1126/science.abb7269 (2020).
39 FDA. Decisional Memorandum - Neutralization titer. (2020).
40 Schwarz, G. Estimating the Dimension of a Model. *The Annals of Statistics* **6**, 461-464, 464 (1978).
41 Nickbakhsh, S. *et al.* Epidemiology of Seasonal Coronaviruses: Establishing the Context for the Emergence of Coronavirus Disease 2019. *J Infect Dis* **222**, 17-25, doi:10.1093/infdis/jiaa185 (2020).
42 Lepiller, Q. *et al.* High incidence but low burden of coronaviruses and preferential associations between respiratory viruses. *J Clin Microbiol* **51**, 3039-3046, doi:10.1128/jcm.01078-13 (2013).
43 Zurich, C. o. *Numbers and facts on COVID-19 [Kanton Zürich. Zahlen & Fakten zu COVID-19]*, < https://www.zh.ch/de/gesundheit/coronavirus/zahlen-fakten-covid-19.html?keyword=covid19#/home (accessed mar 30, 2021)> (

875 44 Bartsch, Y. C. *et al.* Discrete SARS-CoV-2 antibody titers track with functional humoral
876 stability. *Nat Commun* **12**, 1018, doi:10.1038/s41467-021-21336-8 (2021).
877 45 Stephenson, K. E. *et al.* Immunogenicity of the Ad26.COV2.S Vaccine for COVID-19. *JAMA*,
878 doi:10.1001/jama.2021.3645 (2021).
879 46 Alter, G. *et al.* Collaboration between the Fab and Fc contribute to maximal protection
880 against SARS-CoV-2 following NVX-CoV2373 subunit vaccine with Matrix-M vaccination. *Res*
881 *Sq*, doi:10.21203/rs.3.rs-200342/v1 (2021).
882 47 Garcia-Beltran, W. F. *et al.* Multiple SARS-CoV-2 variants escape neutralization by vaccine-
883 induced humoral immunity. *Cell*, doi:10.1016/j.cell.2021.03.013 (2021).
884 48 Aydillo, T. *et al.* Immunological imprinting of the antibody response in COVID-19 patients.
885 *Nat Commun* **12**, 3781, doi:10.1038/s41467-021-23977-1 (2021).
886 49 Jiang, X. L. *et al.* Lasting antibody and T cell responses to SARS-CoV-2 in COVID-19 patients
887 three months after infection. *Nat Commun* **12**, 897, doi:10.1038/s41467-021-21155-x (2021).
888 50 Breton, G. *et al.* Persistent cellular immunity to SARS-CoV-2 infection. *J Exp Med* **218**,
889 doi:10.1084/jem.20202515 (2021).
890 51 Dan, J. M. *et al.* Immunological memory to SARS-CoV-2 assessed for up to 8 months after
891 infection. *Science* **371**, doi:10.1126/science.abf4063 (2021).
892 52 Song, G. *et al.* Cross-reactive serum and memory B cell responses to spike protein in SARS-
893 CoV-2 and endemic coronavirus infection. *bioRxiv*, doi:10.1101/2020.09.22.308965 (2020).
894 53 Anderson, E. M. *et al.* Seasonal human coronavirus antibodies are boosted upon SARS-CoV-2
895 infection but not associated with protection. *Cell*, doi:10.1016/j.cell.2021.02.010 (2021).
896 54 Marot, S. *et al.* Rapid decline of neutralizing antibodies against SARS-CoV-2 among infected
897 healthcare workers. *Nature Communications* **12**, 844, doi:10.1038/s41467-021-21111-9
898 (2021).
899 55 Wei, X. *et al.* Emergence of Resistant Human Immunodeficiency Virus Type 1 in Patients
900 Receiving Fusion Inhibitor (T-20) Monotherapy. *Antimicrobial Agents and Chemotherapy* **46**,
901 1896-1905, doi:10.1128/aac.46.6.1896-1905.2002 (2002).
902 56 Liechti, T. *et al.* Development of a high-throughput bead based assay system to measure HIV-
903 1 specific immune signatures in clinical samples. *J Immunol Methods* **454**, 48-58,
904 doi:10.1016/j.jim.2017.12.003 (2018).
905 57 Breiman, L. Random Forests. *Machine Learning* **45**, 5-32, doi:10.1023/A:1010933404324
906 (2001).
907 58 Liaw, A. a. W., Matthew. Classification and Regression by randomForest. *R News* (2002).
908 59 Team, R. C. (R Foundation for Statistical Computing, Vienna, Austria, 2020).
909 60 Wright, M. N. & Ziegler, A. ranger: A Fast Implementation of Random Forests for High
910 Dimensional Data in C++ and R. *2017* **77**, 17, doi:10.18637/jss.v077.i01 (2017).
911 61 <https://github.com/chlpasin/SARS-CoV-2-serology> (
912 62 Fraser, C. *et al.* Modeling the long-term antibody response of a human papillomavirus (HPV)
913 virus-like particle (VLP) type 16 prophylactic vaccine. *Vaccine* **25**, 4324-4333,
914 doi:10.1016/j.vaccine.2007.02.069 (2007).
915 63 Kuznetsova, A., Brockhoff, P. B. & Christensen, R. H. B. lmerTest Package: Tests in Linear
916 Mixed Effects Models. *2017* **82**, 26, doi:10.18637/jss.v082.i13 (2017).
917 64 Wickham, H. *ggplot2: Elegant Graphics for Data Analysis*. (2016).
918 65 Gu, Z., Eils, R. & Schlesner, M. Complex heatmaps reveal patterns and correlations in
919 multidimensional genomic data. *Bioinformatics* (2016).
920 66 Pasin, C. Multifactorial seroprofiling dissects the contribution of pre-existing human
921 coronaviruses responses to SARS-CoV-2 immunity (SARS-CoV-2-serology: v1.0.0). *Zenodo*,
922 doi:10.5281/zenodo.5588023 (2021).

923

924

Acknowledgments

This work was supported by a grant of the Pandemiefonds of the University of Zurich Foundation to A.T., a grant of the Swiss Red Cross to B.F. and A.T., a grant of the University Hospital Zurich Innovation Grant to M.G.M., the Swiss National Science Foundation grant 31CA30_196906 to H.F.G., A.T., R.K. and the Gilead COVID-19 RFP Research Program COMMIT Grant #: IN-SW-983-6078 (to H.F.G., A.T., R.K.). I.A.A. is supported by a research grant of the Promedica Foundation. Roche Diagnostics supported the study with providing test material for a proportion of the Elecsys S tests.

We thank the staff of the Institute of Medical Virology diagnostics unit, sample triage and administration for their support and the staff of the participating clinics for coordinating the sample collection in the frame of the included clinical trials.

Author Contributions

I.A.A., C.P., M.S., A.T., H.F.G. and R.D.K. conceived and designed the study and analyzed data. I.A.A., M.S., M.M.S., S.E., M.C.H., L.M., M.E.S., A.H., A.A., C.R.N., J.B., M.H. designed and performed binding antibody experiments. P.R., J.W. and S.E. conducted neutralization experiments and analyzed data. S.S. developed an analysis app. C.P. and R.D.K. analyzed data. D.L.B., M.M., A.W., S.K.R., B.M.F., E.S., J.G., C.B., P.M.M.S., M.G.M., H.F.G., A.W., U.K., J.B. and M.H. were involved in patient recruitment, provided samples from study and diagnostic repositories and analyzed patient data. A.T., I.A.A., C.P. and M.S. wrote the manuscript, which all co-authors commented on.

Competing interests

The authors declare no competing financial or non-financial interests.

952 **Figure legends**

953 **Fig. 1. Seroprofiling SARS-CoV-2 responses.** (a) Assessment of the multiplex SARS-CoV-2 ABCORA 2.0
954 on the indicated training (N= 823) and validation (N= 635) cohorts (Supplementary Table 3). Depicted
955 are MFI signals normalized to empty bead controls (MFI-FOE). Grey boxes indicate values above the
956 individually set MFI-FOE cut-offs for SARS-CoV-2 specific responses for each antigen (see
957 Supplementary Table 4). Boxplots represent the following: median with the middle line, upper and
958 lower quartiles with the box limits, 1.5x interquartile ranges with the whiskers. (b) Heatmap
959 representing the measured MFI-FOE values and the outcomes predicted with ABCORA 2.0 - 2.3 of
960 training and validation cohort measurements shown in (a). Negative, Positive, and Positive, partial
961 refer to ranking according to ABCORA 2.0 as specified in Supplementary Table 5. (c) Sensitivity and
962 specificity of ABCORA 2 assay versions based on the combined training and validation cohort data
963 depicted in (a). Proportion of false negative samples (sensitivity; green) and proportion of false positive
964 samples (specificity; blue) are represented by the reduction from 100% (outer circle) per segment. (d)
965 Assessment of ABCORA 2.0 with the National Institute for Biological Standards and Control (NIBSC)
966 Anti SARS-CoV-2 Verification Panel (20/B770) comprising SARS-CoV-2 positive (red) and negative (blue)
967 panel serum samples. Grey boxes indicate values above the ABCORA 2.0 MFI-FOE cut-offs for SARS-
968 CoV-2 specific responses for individual antigen-Ig combinations. Boxplots represent the following:
969 median with the middle line, upper and lower quartiles with the box limits, 1.5x interquartile ranges
970 with the whiskers.

971 **Fig. 2. Quantification of SARS-CoV-2 specific antibody responses.** (a-c) Distribution of (a) 50% effective
972 concentrations (EC50; expressed as reciprocal plasma dilution) and (b) area under the curve values
973 (AUC; expressed as MFI) of titrated plasma from SARS-CoV-2 positive adults (N=72) measured with
974 ABCORA 2.0. (c) Titrated SARS-CoV-2 RBD and S1 responses were quantified using the RBD specific
975 monoclonal antibody CR3022 (produced as IgG, IgA and IgM; expressed as ng/ml) as external standard.
976 See Supplementary Fig. 7 for additional quantification with the WHO International Standard Anti-SARS-
977 CoV-2 Immunoglobulin. (d) Spearman correlation matrix assessing agreement between ABCORA 2.0

978 based quantification readouts (EC50, AUC, RBD Ab standardized), the basic MFI-FOE measured at
979 1/100 plasma dilution (log), indicated summed logMFI-FOE values (1/100 dilution), and Roche Elecsys
980 Anti-SARS-CoV-2 (S) assay results (U/ml). Non-significant correlations are left blank. Levels of
981 significance are assessed by a two-sided test on the asymptotic t approximation of Spearman's rank
982 correlation, and corrected by the Bonferroni method for multiple testing ($p<0.05/780$). Color shading
983 denotes correlation coefficient.

984

985 **Fig. 3. Association of binding and neutralization activity in early and late infection.** (a) 50%
986 Neutralization titers (NT50) titers against Wuhan-Hu-1 pseudotype in patients with known positive
987 SARS-CoV-2 RT-PCR date (N= 369). Patients were stratified according to time since first diagnosis to
988 investigate early (less than 30 days post RT-PCR, lavender) and late (more than 30 days post RT-PCR,
989 turquoise) neutralization responses. Difference between these two groups was assessed with a linear
990 mixed model with time since RT-PCR (binary variable early/late) as fixed effect and individual as
991 random effect and using Satterthwaite approximation for a two-sided t-test on the parameter
992 associated with time since RT-PCR. Boxplots represent the following: median with the middle line,
993 upper and lower quartiles with the box limits, 1.5x interquartile ranges with the whiskers. (b) Linear
994 regression analysis to define association between neutralization (reciprocal NT50) and antibody
995 binding (MFI-FOE). Black lines indicate linear regression predictions and grey shaded areas correspond
996 to the 95% confidence intervals. Results depict early (lavender), late (turquoise) and full cohort (black).
997 n.s. denotes non-significant results. Levels of significance are assessed by a two-sided test on the
998 asymptotic t approximation of Spearman's rank correlation, and corrected by the Bonferroni method
999 for multiple testing ($p<0.05/1200$, see Supplementary Fig. 8b and 9).

1000 **Fig. 4. Predicting neutralization capacity as a function of binding activity.** (a) SARS-CoV-2 positive
1001 donors (N=467) were stratified into high neutralizers (NT50 >250, N=332; blue) and no/low neutralizers
1002 (NT50 <250, N=135; grey), based on their neutralization activity against Wuhan-Hu-1. (b) and (c)
1003 Comparison of the prediction ability of six different classification models using 100 cross-validation

1004 sets (divided as 80% for training and 20% for validation. (b) Comparison of models by area under the
1005 curve (AUC). Each dot corresponds to one cross-validation set. (c) Bayesian information criterion (BIC)
1006 of the five models based on logistic regression. The different models are: Univariable logistic
1007 regressions (ULR). ULR-RBD: mean of MFI-FOE RBD. ULR-S1: mean of MFI-FOE S1. Multivariable logistic
1008 regression (MLR). MLR-S1, RBD: mean of S1 reactivity and mean of RBD reactivity. MLR-PCA2 and MLR-
1009 PCA4: MLR of 2 and 4 first axis of PCA analysis, respectively. PCA was based on all 12 SARS-CoV-2
1010 antibody reactivities measured by ABCORA 2.0. Random forest (RF) including all antibody reactivities
1011 measured by ABCORA 2.0. Boxplots represent the following: median with the middle line, upper and
1012 lower quartiles with the box limits, 1.5x interquartile ranges with the whiskers and outliers with points.
1013 (d) ULR-S1 estimated ROC curve based on full data set (N=467). (e) Measured NT50 value versus
1014 probability of NT50 >250 as predicted by ULR-S1 in five randomly chosen validation sets (each symbol
1015 corresponds to a validation set). Purple colored symbols indicate a higher than 0.70 probability of the
1016 respective sample to be neutralizing at NT50 >250 and are therefore denoted as high neutralizers. Grey
1017 indicates samples with predicted neutralization NT50 <250, therefore classified as no/low neutralizers.
1018 (f) Neutralization prediction based on a modified ULR-S1 model utilizing the diagnostic readout SOC
1019 instead of MFI-FOE values as input. Measured NT50 value versus sum of S1 SOC values (IgG, IgA, IgM)
1020 are depicted. Dashed lines correspond to a NT50=250 horizontally and the sum S1 SOCs=9.7 vertically.
1021 The sum S1 SOCs=9.7 corresponds to the thresholds depicted for ULR-S1 in (d) and (e). The grey shaded
1022 area corresponds to true positives (individuals with NT50 >250 predicted as high neutralizers).

1023 **Fig. 5. Monitoring temporal evolution of antibody responses.** (a) ABCORA 2.3 definition of
1024 seropositivity in donors with positive RT-PCR confirmed SARS-CoV-2 infection and known RT-PCR date
1025 (N=369). Seropositivity rating in relation to plasma sampling time point post diagnosis is depicted. Grey
1026 shaded area highlights the first seven days since positive RT-PCR detection. (b) Power law model, with
1027 time since RT-PCR as fixed effect and individual as random effect, estimating the decay of antibody
1028 binding activity based on ABCORA 2.0 measurements at 1 - 4 longitudinal time points in 120 individuals
1029 totaling in 251 measurements. Purple lines correspond to the models estimation and purple shaded

areas to the 95% confidence intervals. Antibody half-lives (t1/2 in days) from significant models are depicted. Significance was assessed using Satterthwaite approximation for a two-sided t-test on the slope parameters. (c) Power law model, with time since RT-PCR as fixed effect and individual as random effect, estimating the decay of neutralizing capacity on 251 measurements from 120 individuals. Only individuals with NT50>100 at their first measurement were used to estimate the half-life. The purple line corresponds to the model estimation and the purple shaded area to the 95% confidence intervals. Significance was assessed using Satterthwaite approximation for a two-sided t-test on the slope parameters.

Fig. 6. Seasonal and annual fluctuation in HCoV reactivity. Reactivity to human coronaviruses (HCoV-NL63, HCoV-229E, HCoV-HKU1, HCoV-OC43) was compared by ABCORA 5.0. Reactivity in healthy blood donors from 2019 and 2020 was compared. Pre-pandemic samples included: January 2019 (N=285), May 2019 (N=288), January 2020 (N=252). Samples from May 2020 (N=672) were collected during the pandemic in Switzerland. Only samples without SARS-CoV-2 specific reactivity as defined by ABCORA were included (N=653). Stars correspond to levels of significance of two-sided t-tests comparing the indicated groups. Levels of significance are corrected by the Bonferroni method for multiple testing and indicated as follows: *p<0.05/36, **p<0.01/36, ***p<0.001/36. Boxplots represent the following: median with the middle line, upper and lower quartiles with the box limits, 1.5x interquartile ranges with the whiskers and outliers with points.

Fig. 7. Effects of pre-existing HCoV immunity during SARS-CoV-2 acquisition. (a) Time-matched comparison of ABCORA 5.0 reactivity for SARS-CoV-2 and HCoVs in healthy and SARS-CoV-2 infected individuals. Healthy donors were sampled in May 2020 (N=653; blue). Plasma from SARS-CoV-2 infected individuals were collected between April - June 2020 (N=65; red). See Supplementary Fig. 14 for analysis on the full SARS-CoV-2 positive cohort (N=389). Grey boxes indicate values above the individual MFI-FOE cut-offs for SARS-CoV-2 specific responses for each antigen. Stars correspond to levels of significance of two-sided t-tests comparing negative versus positive patients. Levels of significance are corrected by the Bonferroni method for multiple testing and indicated as follows:

1056 *p<0.05/12, **p<0.01/12, ***p< 0.001/12 (IgG HKU1: p=0.66, IgG OC43: p=0.45, IgG NL63: $p=3.3x10^{-}$
1057 ^{04}, IgG 229E: $p=1.6x10^{-05}$, IgA HKU1: $p=1.8x10^{-03}$, IgA OC43: $p=1.3x10^{-05}$, IgA NL63: $p=1.4x10^{-07}$, IgA 229E:
1058 $p=3.0x10^{-05}$, IgM HKU1: $p=3.3x10^{-08}$, IgM OC43: $p=4.3x10^{-03}$, IgM NL63: $p=1.1x10^{-07}$, IgM 229E:
1059 $p=2.7x10^{-02}$). Boxplots represent the following: median with the middle line, upper and lower quartiles
1060 with the box limits, 1.5x interquartile ranges with the whiskers and outliers with points. (b) Linear
1061 regression models showing the association between SARS-CoV-2 and HCoV signals in 204 SARS-CoV-2
1062 positive patients with known dates of first positive RT-PCR detection. Influences within the same
1063 antibody class are investigated. The models were adjusted on age (spline with 3 degrees of freedom),
1064 gender, time since positive RT-PCR (spline with 3 degrees of freedom) and level of HCoV reactivity.
1065 Samples are defined to harbor high HCoV reactivity if they show ABCORA 5.0 HCoV logMFI-FOE values
1066 higher than the corresponding median in at least 3 HCoV measurements (HKU1, OC43, NL63 or 229E).
1067 Curves correspond to the models estimation and shaded areas to the 95% confidence intervals. p-
1068 values were obtained by running a two-sided Student t-test on the parameter associated to HCoV
1069 reactivity in the linear regression. (c) Linear regression model showing the association between SARS-
1070 CoV-2 IgG and HCoV IgA signals. Curves correspond to the models estimation and shaded areas to the
1071 95% confidence intervals. p-values were obtained by running a two-sided Student t-test on the
1072 parameter associated to HCoV reactivity in the linear regression. (d) Linear regression model showing
1073 the association between SARS-CoV-2 IgG and HCoV IgM signals. Curves correspond to the models
1074 estimation and shaded areas to the 95% confidence intervals. p-values were obtained by running a
1075 two-sided Student t-test on the parameter associated to HCoV reactivity in the linear regression.

1076 **Fig. 8. Impact of HCoV immunity on COVID-19 severity.** (a) Association of hospitalization status (not
1077 hospitalized (N=16); hospitalized not in ICU (N=42); hospitalized in ICU (N=22)) and high or low IgG
1078 HCoV reactivity. Rectangle sizes correspond to the proportion of included patients. (b) Influence of
1079 HCoV reactivity (low/high) on the hospitalization status in a subset of N=80 patients, as estimated with
1080 odds ratios, in an ordinal regression (with levels=not hospitalized (N=16); hospitalized not in ICU
1081 (N=42); hospitalized in ICU (N=22)) and a logistic regression (reference=not hospitalized (N=16); versus

all hospitalized (N=64)). Data is presented as parameter estimation and its 95% confidence interval. Level of significance of the parameter is obtained with a two-sided t-test (p-value is displayed if <0.05, otherwise indicated as n.s.).

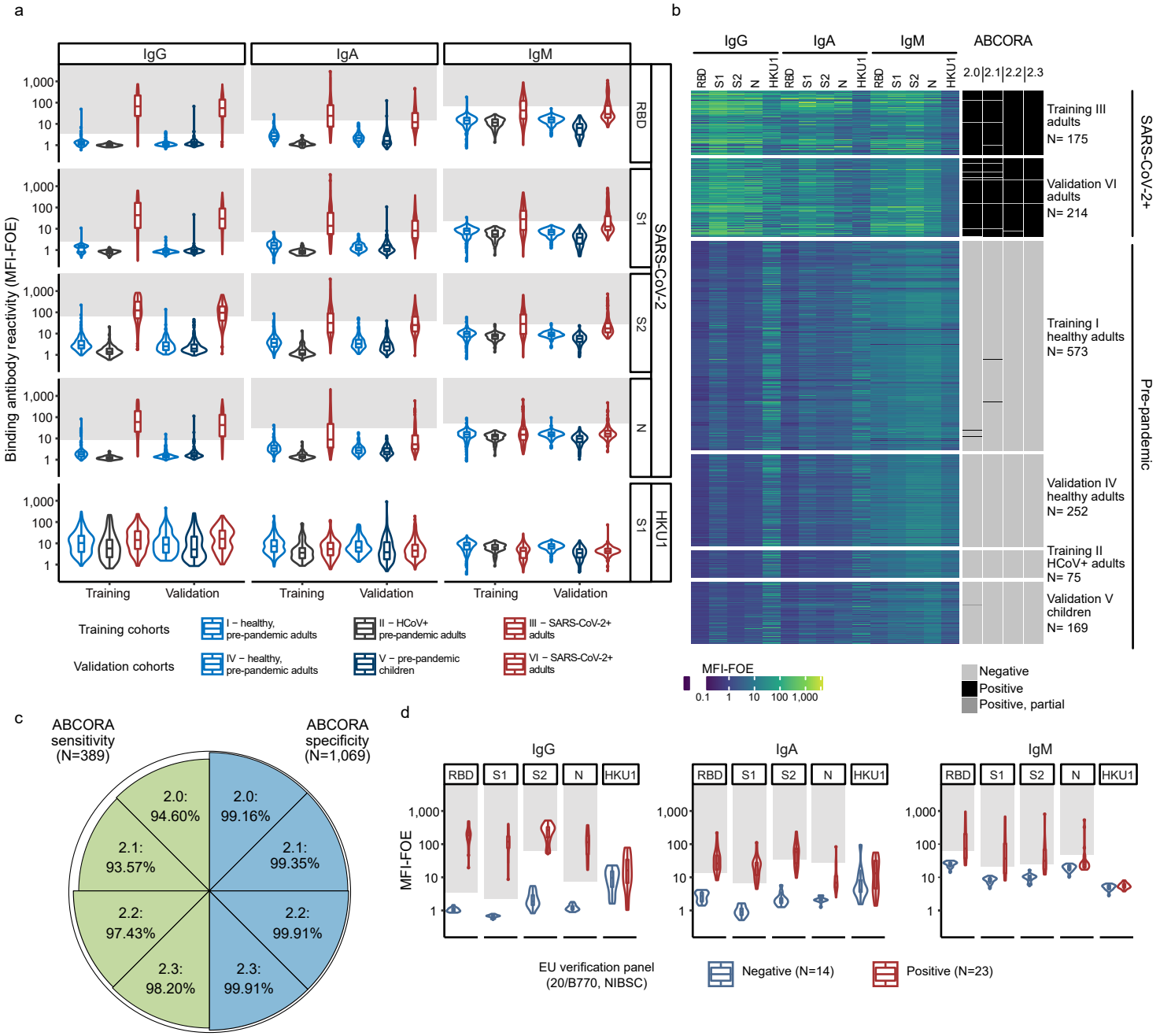
a
IgG
IgA
IgM
RBD
S1
S2
N
HKU1
SARS-CoV-2
Binding antibody reactivity (MFI-FOE)
1,000
100
10
1
Training
Validation
Training cohorts
I – healthy, pre-pandemic adults
II – HCoV+ pre-pandemic adults
III – SARS-CoV-2+ adults
Validation cohorts
IV – healthy, pre-pandemic adults
V – pre-pandemic children
VI – SARS-CoV-2+ adults
b
ABCORA
2.0
2.1
2.2
2.3
Training III adults N= 175
Validation VI adults N= 214
Training I healthy adults N= 573
Validation IV healthy adults N= 252
Training II HCoV+ adults N= 75
Validation V children N= 169
SARS-CoV-2+
Pre-pandemic
MFI-FOE
0.1
1
10
100
1,000
Negative
Positive
Positive, partial
c
ABCORA sensitivity (N=389)
ABCORA specificity (N=1,069)
2.0: 94.60%
2.0: 99.16%
2.1: 93.57%
2.1: 99.35%
2.2: 97.43%
2.2: 99.91%
2.3: 98.20%
2.3: 99.91%
d
MFI-FOE
EU verification panel (20/B770, NIBSC)
Negative (N=14)
Positive (N=23)

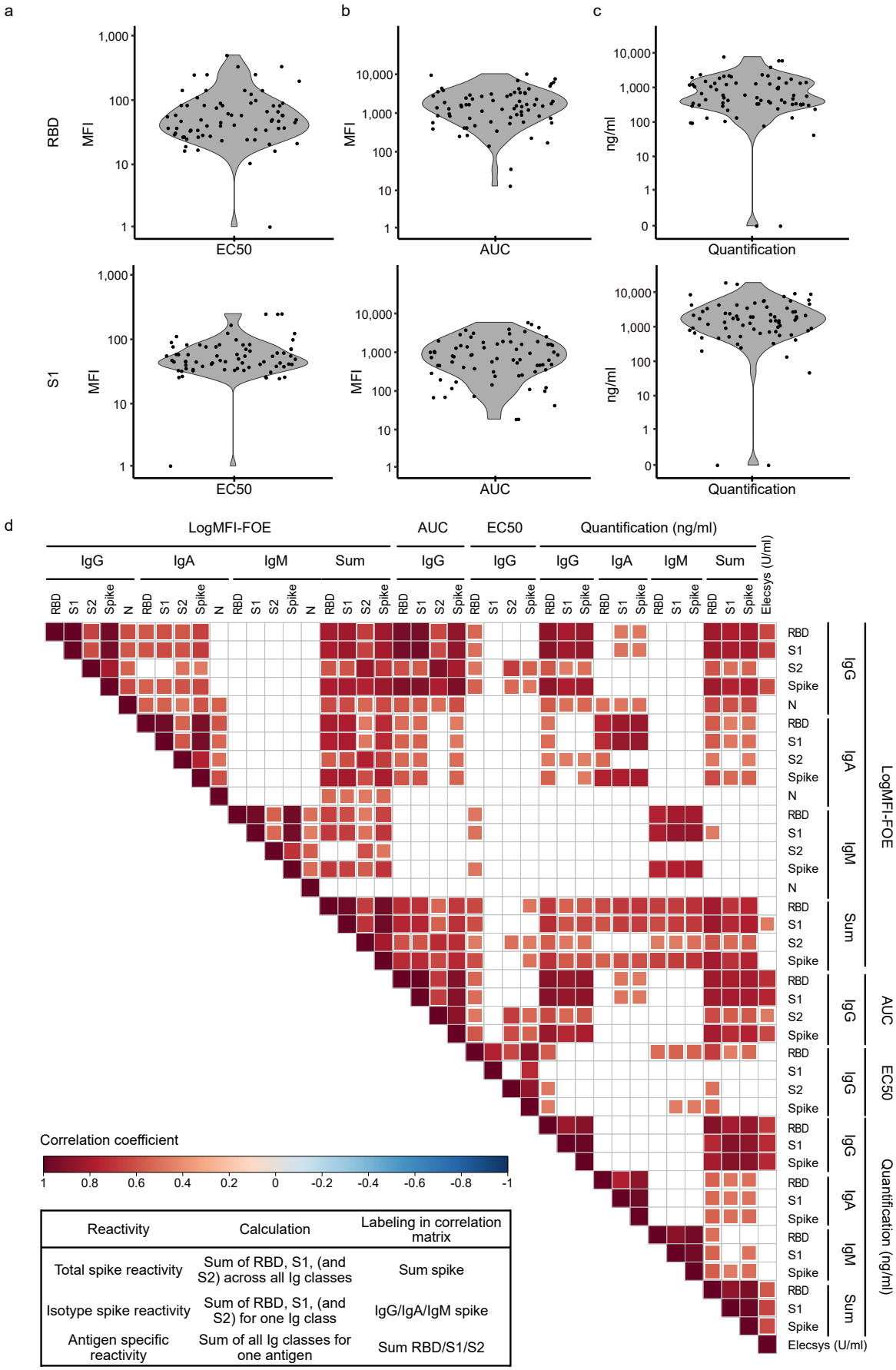

Reactivity	Calculation	Labeling in correlation matrix
Total spike reactivity	Sum of RBD, S1, (and S2) across all Ig classes	Sum spike
Isotype spike reactivity	Sum of RBD, S1, (and S2) for one Ig class	IgG/IgA/IgM spike
Antigen specific reactivity	Sum of all Ig classes for one antigen	Sum RBD/S1/S2

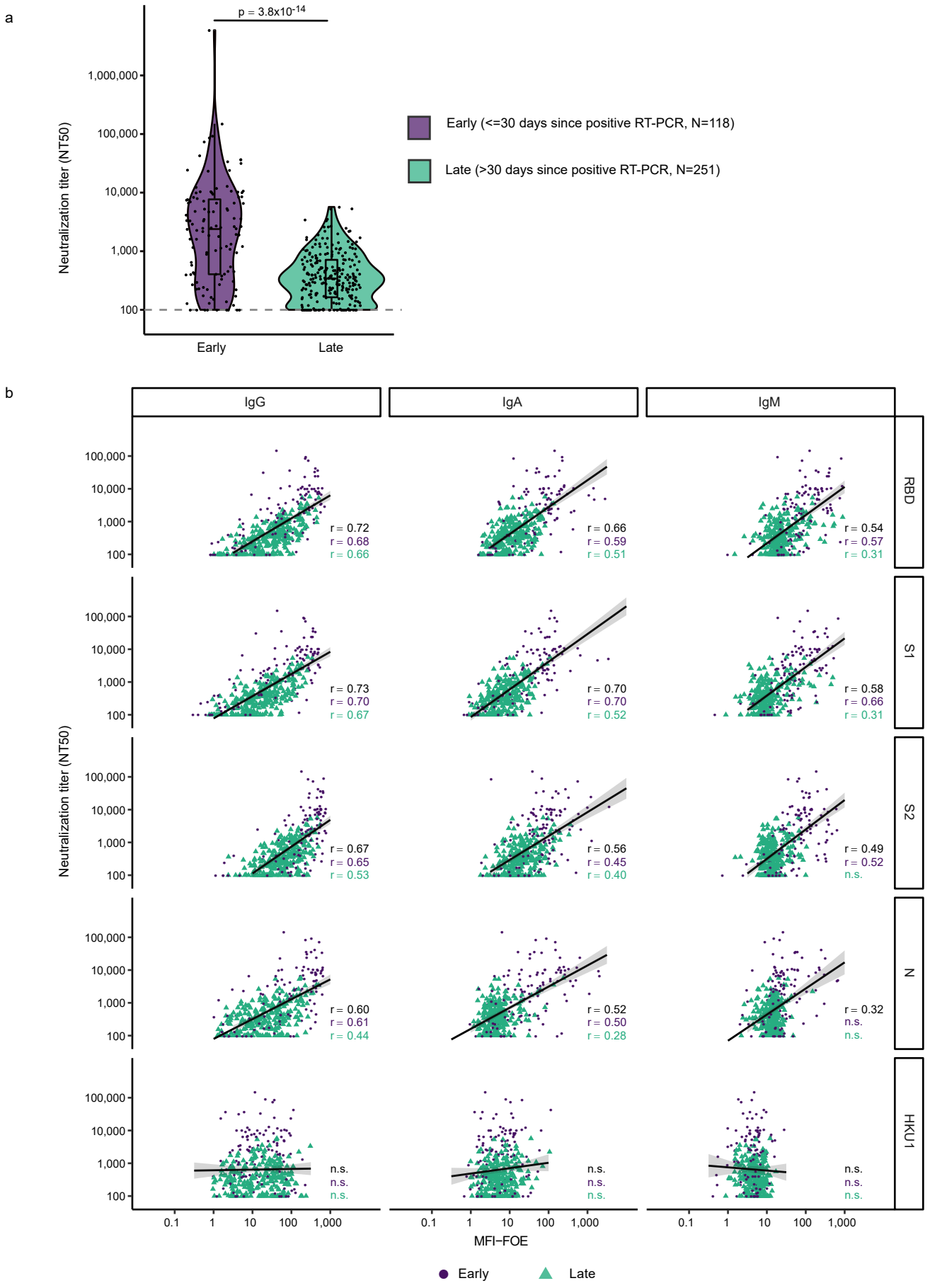
a
p = 3.8x10-14
Neutralization titer (NT50)
1,000,000
100,000
10,000
1,000
100
Early
Late
Early (<=30 days since positive RT-PCR, N=118)
Late (>30 days since positive RT-PCR, N=251)
b
IgG
IgA
IgM
RBD
S1
S2
N
HKU1
r = 0.72
r = 0.68
r = 0.66
r = 0.66
r = 0.59
r = 0.51
r = 0.54
r = 0.57
r = 0.31
r = 0.73
r = 0.70
r = 0.67
r = 0.70
r = 0.70
r = 0.52
r = 0.58
r = 0.66
r = 0.31
r = 0.67
r = 0.65
r = 0.53
r = 0.56
r = 0.45
r = 0.40
r = 0.49
r = 0.52
n.s.
r = 0.60
r = 0.61
r = 0.44
r = 0.52
r = 0.50
r = 0.28
r = 0.32
n.s.
n.s.
n.s.
n.s.
n.s.
n.s.
n.s.
n.s.
n.s.
n.s.
0.1
1
10
100
1,000
MFI−FOE
Early
Late

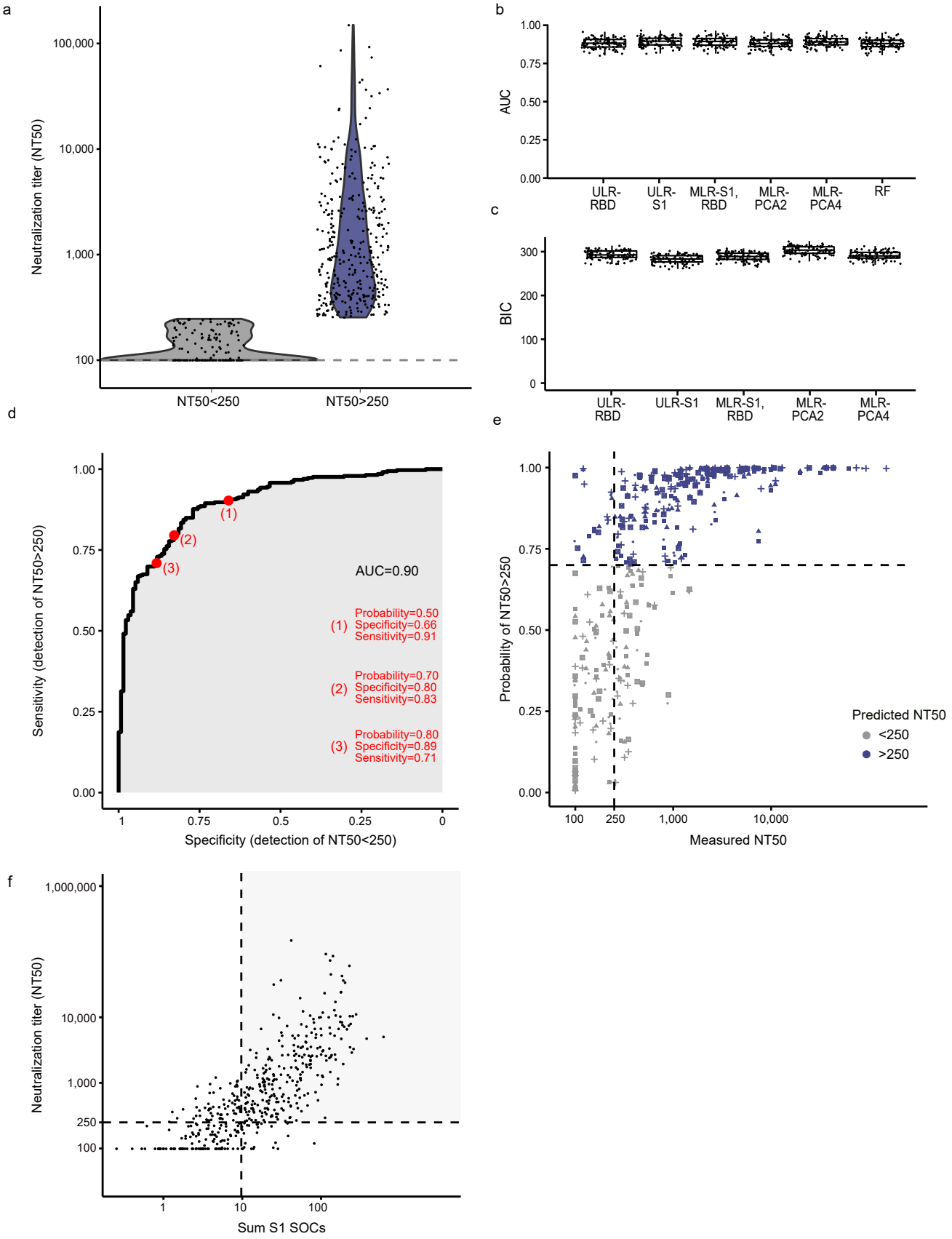
a
Neutralization titer (NT50)
100,000
10,000
1,000
100
NT50<250
NT50>250
b
AUC
1.00
0.75
0.50
0.25
0.00
ULR-RBD
ULR-S1
MLR-S1, RBD
MLR-PCA2
MLR-PCA4
RF
c
BIC
300
200
100
0
ULR-RBD
ULR-S1
MLR-S1, RBD
MLR-PCA2
MLR-PCA4
d
Sensitivity (detection of NT50>250)
Specificity (detection of NT50<250)
AUC=0.90
(1)
(2)
(3)
(1) Probability=0.50 Specificity=0.66 Sensitivity=0.91
(2) Probability=0.70 Specificity=0.80 Sensitivity=0.83
(3) Probability=0.80 Specificity=0.89 Sensitivity=0.71
e
Probability of NT50>250
Measured NT50
100
250
1,000
10,000
Predicted NT50
<250
>250
f
Neutralization titer (NT50)
1,000,000
10,000
1,000
250
100
1
10
100
Sum S1 SOCs

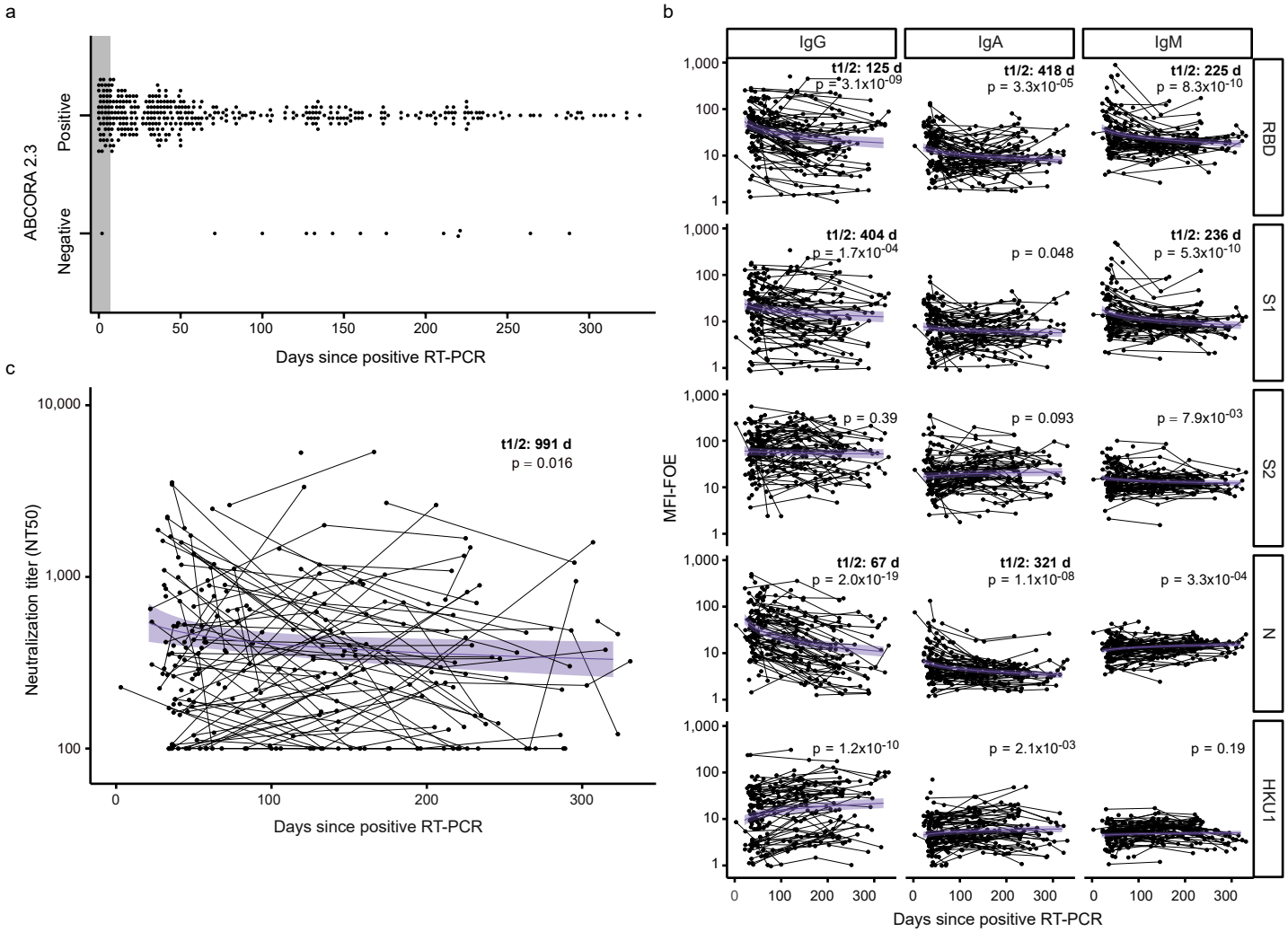
a
ABCORA 2.3
Positive
Negative
0
50
100
150
200
250
300
Days since positive RT-PCR
b
IgG
IgA
IgM
RBD
S1
S2
N
HKU1
MFI-FOE
1,000
100
10
1
t1/2: 125 d
p = 3.1x10-09
t1/2: 418 d
p = 3.3x10-05
t1/2: 225 d
p = 8.3x10-10
t1/2: 404 d
p = 1.7x10-04
p = 0.048
t1/2: 236 d
p = 5.3x10-10
p = 0.39
p = 0.093
p = 7.9x10-03
t1/2: 67 d
p = 2.0x10-19
t1/2: 321 d
p = 1.1x10-08
p = 3.3x10-04
p = 1.2x10-10
p = 2.1x10-03
p = 0.19
0
100
200
300
Days since positive RT-PCR
c
Neutralization titer (NT50)
10,000
1,000
100
t1/2: 991 d
p = 0.016
0
100
200
300
Days since positive RT-PCR

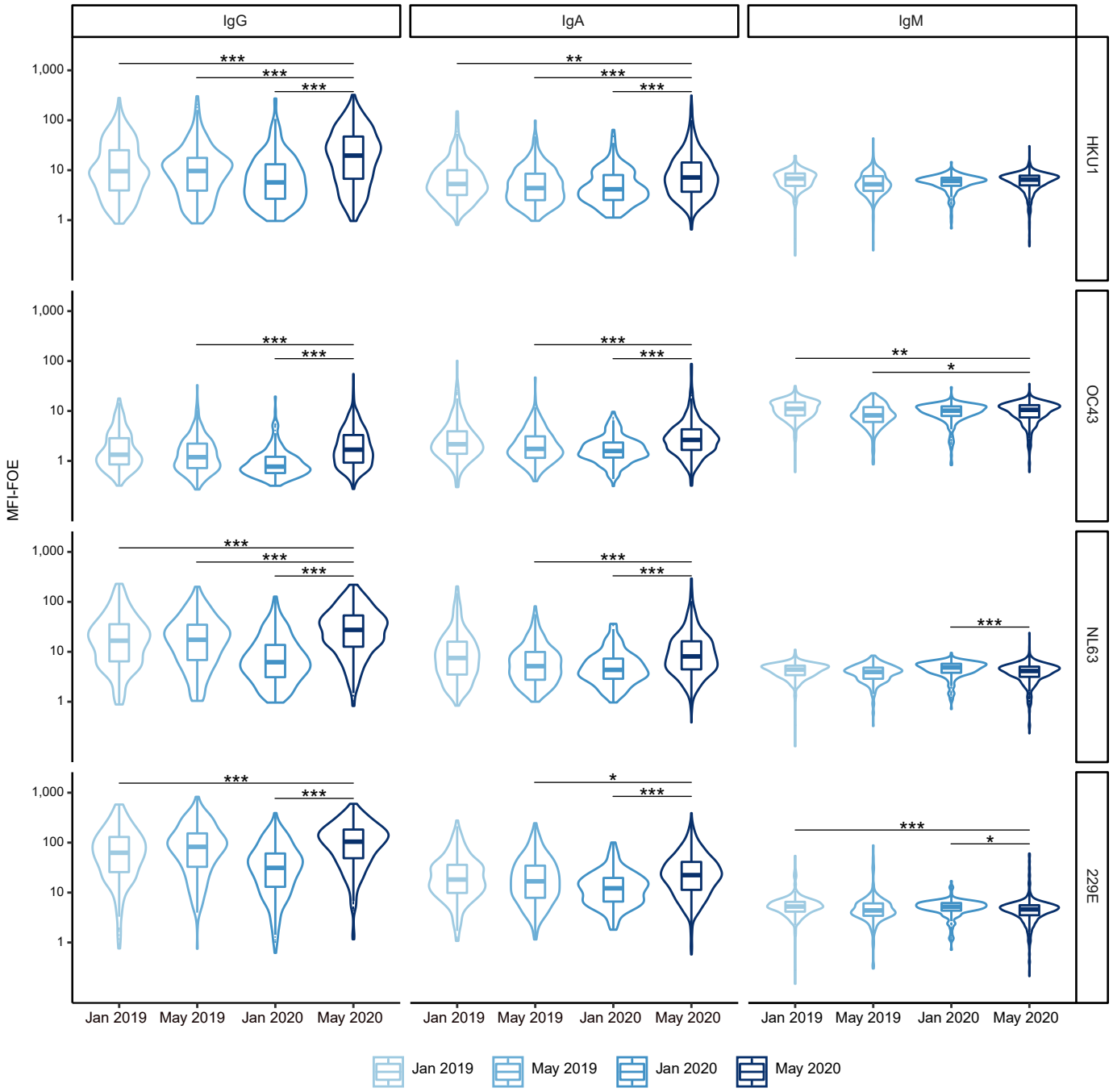
IgG
IgA
IgM
HKU1
OC43
NL63
229E
MFI-FOE
1,000
100
10
1
***
**
*
Jan 2019
May 2019
Jan 2020
May 2020

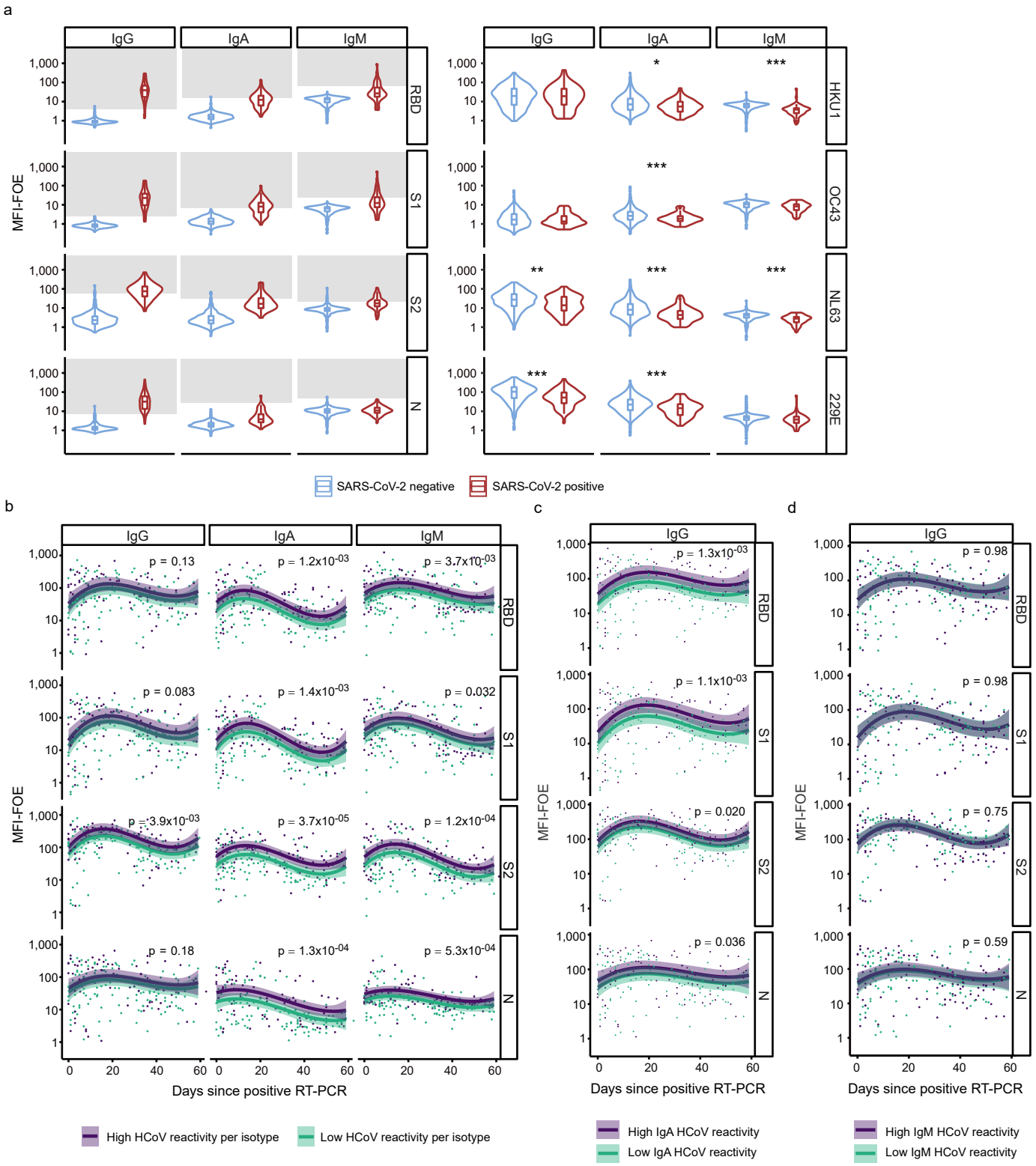
a
IgG
IgA
IgM
RBD
S1
S2
N
HKU1
OC43
NL63
229E
MFI-FOE
1,000
100
10
1
*
***
**
SARS-CoV-2 negative
SARS-CoV-2 positive
b
p = 0.13
p = 1.2x10-03
p = 3.7x10-03
p = 0.083
p = 1.4x10-03
p = 0.032
p = 3.9x10-03
p = 3.7x10-05
p = 1.2x10-04
p = 0.18
p = 1.3x10-04
p = 5.3x10-04
0
20
40
60
Days since positive RT-PCR
High HCoV reactivity per isotype
Low HCoV reactivity per isotype
c
p = 1.3x10-03
p = 1.1x10-03
p = 0.020
p = 0.036
High IgA HCoV reactivity
Low IgA HCoV reactivity
d
p = 0.98
p = 0.98
p = 0.75
p = 0.59
High IgM HCoV reactivity
Low IgM HCoV reactivity

a

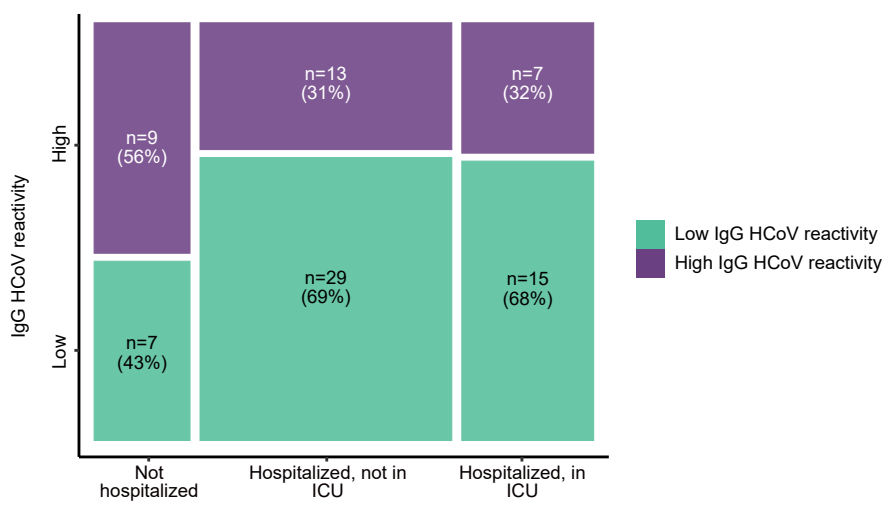
IgG HCoV reactivity
High
Low
n=9
(56%)
n=7
(43%)
n=13
(31%)
n=29
(69%)
n=7
(32%)
n=15
(68%)
Not hospitalized
Hospitalized, not in ICU
Hospitalized, in ICU
Low IgG HCoV reactivity
High IgG HCoV reactivity

b

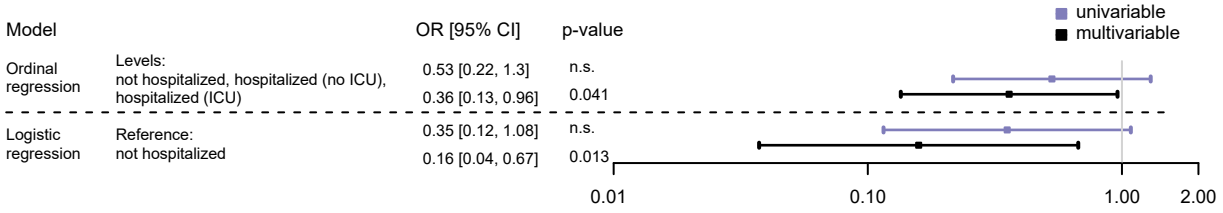
Model
OR [95% CI]
p-value
univariable
multivariable
Ordinal regression
Levels:
not hospitalized, hospitalized (no ICU), hospitalized (ICU)
0.53 [0.22, 1.3]
n.s.
0.36 [0.13, 0.96]
0.041
Logistic regression
Reference:
not hospitalized
0.35 [0.12, 1.08]
n.s.
0.16 [0.04, 0.67]
0.013
0.01
0.10
1.00
2.00